

Master's Thesis

# Studies of vacuum discharges in the CLIC accelerating structure

Anton Tropp

In cooperation with  
Department of Physics and Astronomy,  
Uppsala University

Department of Electrical and Information Technology,  
Faculty of Engineering, LTH, Lund University, 2016.



FACULTY OF ENGINEERING - LTH

MASTER'S THESIS

---

**Studies of vacuum discharges in the CLIC  
accelerating structure**

---

*Author:*  
Anton Tropp, Lund University

June 17, 2016

*Supervisor:*  
Anders Karlsson, Lund University  
*Assistant Supervisor*  
Marek Jacewicz, Uppsala University

### **Abstract**

The Compact Linear Collider (CLIC), is one of the proposed successors to the Large Hadron Collider (LHC) accelerator at the European Organization for Nuclear Research. (CERN). In CLIC, particles are accelerated by very strong electric fields. Unfortunately, large electric fields may lead to vacuum discharges, which in turn can affect the particle beam by disrupting the flow of energy inside the accelerating structure and deteriorate the performance of the accelerator. Studies of the physics of vacuum discharges and its effect on the beam are crucial for the realization of the CLIC accelerator.

The objective of this master thesis is to improve the knowledge of how vacuum discharges occur and what can be done to prevent them. The project was done together with the CLIC group at Uppsala University. They have their diagnostic equipment, Uppsala/CLIC X-band spectrometer (UCXS), at the High Gradient Test Stand for research on RF-structures X-Box2, where also the accelerating structure is located. The spectrometer consists of a collimator, a dipole and a fluorescent screen, which receives images from electrons that come from discharges. These images have been analysed, together with Radio Frequency (RF)-signal data from X-Box2, to find discharge positions inside the accelerating structure. The achieved results are consistent with previous analyses used with the help of the RF signals. We see that there is a possibility to use images to study the geometrical shape of the discharges. Longitudinal positioning of the discharges with the help of images, cannot be done. While longitudinal positioning cannot be done, transversal have had success and can be found. Images have also been seen with multiple features. It is hard to accredit one image to a single breakdown and a hypothesis is that there are more than one breakdown during a pulse, creating multiple features.

# Contents

<b>1</b>	<b>Introduction</b>	<b>4</b>
<b>2</b>	<b>Theory and Background</b>	<b>5</b>
2.1	CLIC	5
2.1.1	CLIC design and problems	6
2.1.2	CTF3	9
2.1.3	Cavities	9
2.1.4	Conditioning	11
2.1.5	X-Box	12
2.2	Vacuum Discharges	14
<b>3</b>	<b>Instrumental Set-Up</b>	<b>15</b>
3.1	X-Box2	15
3.2	Uppsala spectrometer	17
<b>4</b>	<b>Data Analysis</b>	<b>18</b>
4.1	Data format	18
4.2	Data Conversion	20
4.3	Breakdown Positioning	21
4.4	Longitudinal Methods	21
4.4.1	Edge Method	21
4.4.2	Correlation Method	23
4.4.3	Faraday-Cup Method [FC-Method]	24
4.4.4	Phase method	26
4.5	UCXS Images	27
4.5.1	Image Calibration	28
<b>5</b>	<b>Results</b>	<b>36</b>
5.1	Results Longitudinal Methods	36
5.1.1	Edge Method	36
5.1.2	Correlation Method	37
5.1.3	Faraday cup Method	38
5.1.4	Difference	39
5.2	Results from UCXS Images	41
5.2.1	Features	41
5.2.2	RF-Signals	42
5.2.3	Multiple Features	43
<b>6</b>	<b>Summary and Outlook</b>	<b>50</b>
6.1	Conclusion Breakdown Positioning	50
6.1.1	RF-Positioning	50
6.1.2	Image analysis	50
6.2	Future Work	51
6.2.1	Improvements	51
6.3	Contribution	51

<b>7 Acknowledgments</b>	<b>52</b>
7.1 Acknowledgments . . . . .	52
<b>Appendices</b>	<b>53</b>
.1 Appendix A . . . . .	54
.2 Appendix B . . . . .	59

## ACRONYMS

<b>BDR</b>	Breakdown Rate
<b>BLM</b>	Beam Loss Monitor
<b>CERN</b>	European Organization for Nuclear Research.
<b>CLIC</b>	Compact Linear Collider
<b>CTF3</b>	CLIC Test Facility
<b>FEL</b>	Free electron laser
<b>FPGA</b>	Field-programmable gate array
<b>ILC</b>	International Linear Collider
<b>IP</b>	Interaction Point
<b>KEK</b>	The High Energy Accelerator Research Organization, Tsukuba, Japan
<b>LHC</b>	Large Hadron Collider
<b>Linac</b>	Linear Accelerator
<b>LLRF</b>	Low Level Radio Frequency
<b>PETS</b>	Power Extraction Transfer Structure
<b>RF</b>	Radio Frequency
<b>SLAC</b>	Stanford National Accelerator Laboratory
<b>TBTS</b>	Two beam Test Stand
<b>TWT</b>	Travelling Wave Tube
<b>UCXS</b>	Uppsala/CLIC X-band spectrometer
<b>X-Box</b>	High Gradient Test Stand for research on RF-structures

# Chapter 1

## Introduction

This report is part of the graduation for a M.Sc in physics, with focus on accelerator science at the University of Lund, faculty of engineering (Sweden). The work was done at the department of Physics and Astronomy, Uppsala University, during the period February-June 2016.

The goal of this thesis was to find a way to further increase the knowledge about breakdowns inside high gradient structures. With the help of the X-Box2 setup and the UCXS data was received. New and different methods were tried for localisation of breakdown positions. Comparisons between these methods was to be done to see if they resembled earlier results and to see if more information to why they differed could be found. Images from the UCXS was used to first of all see if breakdown positions, both longitudinal and transversal, could be found from the calculated sizes of the image spots. It was also of interest to try and characterize different features seen on the images.

Electrical discharges is a well-known physics phenomena. These discharges have for a long time been a problem when dealing with high electrical fields. With the increasing demand for higher energies for further research and development in high energy physics, there is a need for higher gradient structures. As for accelerators an increased gradient means lower cost and length of the tunnel. However, in accelerators, electrical vacuum breakdowns or breakdowns makes it difficult to reach these super high gradients. CLIC will reach a loaded gradient of 100 MV/m, which is about three times as high as the usual linear accelerators. Superconducting technologies cannot reach these gradients. This makes the concept of having a normal conducting structure more attractive due to the shorter length for the same energy, all this with the cost of having shorter pulses to reach high enough power without losing too much energy and destroy the structure. When a breakdown occurs it can disrupt the energy transfer to the beam and damage the structure.

To be able to understand the physics behind breakdowns inside the vacuum structure of an accelerator the CLIC Test Facility (CTF3) collaboration has started projects regarding this matter. Multiple test facilities and stands have been constructed to create an opportunity for research and development of technology that can make high gradient structures work better and more efficiently.

This thesis will be divided into five chapters and one Acknowledgement chapter after this introduction. Chapter 2 explains breakdown physics and where studies is done together with some background. Chapter 3 will go into details about the instrument setup used during the work period of this thesis. This includes a detailed explanation of the UCXS together with the test stand X-Box2 where all data and images comes from. The fourth chapter 4 explains the author's analysis and how this can be helpful in understanding of the vacuum breakdown phenomena and for future studies of breakdown physics. Chapter 5 explain results from the data analysis. Last chapter 6 gives an outlook as well as a summary/discussion to what have been seen and how this work can be used in the future.

## Chapter 2

# Theory and Background

This chapter will present the basics of the CLIC project with regards to the CTF3 collaboration. Projects such as the Two beam Test Stand (TBTS) and the High Gradient Test Stand for research on RF-structures (X-Box) project will briefly be described. Theory about vacuum breakdowns will shortly be presented with suggested articles for further reading.

### 2.1 CLIC

The CLIC facility is in its concept phase and might not even be constructed, see section 2.1.1. The feasibility of CLIC is well demonstrated by a lot of different studies and new technologies but problems still exist, see [1, p.763]. The CLIC project will find more information regarding the field of high energy particle physics, especially due to the high interest coming from the discovery of the Higgs boson. By creating a collision between an electron and a positron a total energy of 3 TeV is the energy aim for the project. This energy is lower than the energy of the already working collider LHC. However there is a fundamental difference between colliding leptons (electrons/-positrons) as for CLIC and hadrons(protons) as for LHC. Hadrons is composed of quarks while leptons are single point particles, this makes the energy in a collision very different because of how much energy that can be used to create new particles instead of being absorbed by particles we already know is there. This physical difference will make Hadrons very good particles for scanning energies while trying to understand at what energy we can find something new, while Leptons will be much better for precision measurements when we know the energy required. This means that CLIC will be a complement for LHC but with measurements at a much higher accuracy.

In figure 2.1 we can see an illustration for how CLIC can be constructed together with a legend over the different stages of construction. Instead of constructing the total length of about 48.3 km at once, the construction can use energy related key steps. This means that a smaller sites can first be constructed to incorporate the newly interesting 380 GeV peak seen by LHC. This first step was just recently changed and is of yet not fully decided since the first energy point was earlier set to be 500 GeV. Second stage would be an extension to reach 1.5 TeV, to then if necessary extend it to the full length reaching an energy of 3 TeV.



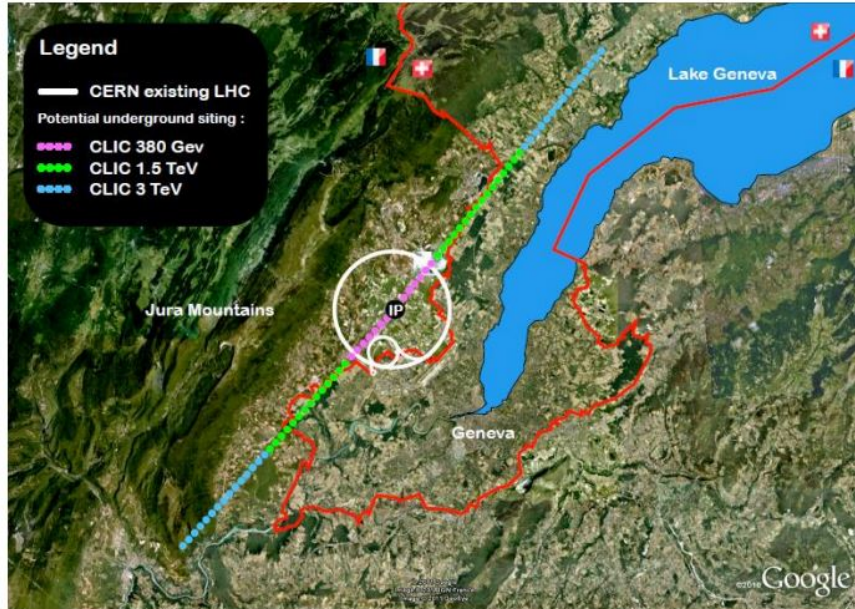


Figure 2.1: Illustration over a possible location and energy stage plan for CLIC. From [14]

### 2.1.1 CLIC design and problems

We can see the CLIC schematic in figure 2.2 together with some of its parameters in table 2.1. In the schematic we can see that CLIC will use a two beam scheme. The concept of having a secondary beam power the main beam is a new technology created for the CLIC project. The first accelerating part, the main beam is the one that by dampening rings generate a beam with low emittance. This beam will further be transported into the main linac structure and can be seen in the lower part of the figure. Emittance is a parameter used to describe the beam and depends on the beam size in both transversal directions together with the beta function. The beta function is the amplitude of the oscillation of the beam. The second beam is what makes the 100 MV/m possible. Here a second beam is generated, which will power the main beam with the necessary RF power. Usually linac structures are powered by klystrons but in this case, klystrons would not be a feasible investment. It would require a total number of about 35 000 high power klystrons which is unreasonable out of an economic perspective. Superconducting technologies will not be used since it cannot achieve the 100 MV/m that is needed. The International Linear Collider (ILC) is a project with the same purpose as CLIC but will use superconducting technology. ILC with about the same length reaches an energy of 1.5 TeV with a gradient of 35 MV/m. This makes the interest for CLIC bigger but all problems with CLIC have not yet been solved.

Table 2.1: Table with CLIC parameters, from [1]

Energy	380 GeV, 1500 GeV, 3000 GeV
Length (proposed)	48.3 kM
Luminosity	$5.9 \times 10^{34}/cm^2 s$
Gradient	100 MV/m
Repetition rate	50 Hz
Nr of particles per bunch	$3.72 \times 10^9$
Nr of bunches per pulse	312
Bunch length	156 ns
Pulse length	200 ns
Frequency	11.994 GHz
$Emittance_x$	600 nm rad (at linac injection point)
$Emittance_y$	10 nm rad (at linac injection point)

The energy transfer from drive beam to main beam is done by a structure called Power Extraction Transfer Structure (PETS). PETS's power the accelerator structures all the way to the Interaction Point (IP) and work by having the fields of incoming electrons captured by the structure geometry. This field will then start to resonate at the structure frequency. This makes it possible to work as a RF source transferring power to the main beam if the frequency is the 12 GHz needed for CLIC. It is important that this process works well and is optimized correctly with phase and frequency for the acceleration to work as intended. The transfer efficiency is 93.8 % from the PETS to the accelerating structure which is impressive due to the high precision monitoring needed for a good transfer, from [1, p.9-10].

CLIC has been in design phase for a few decades already and this is due to both the size of the project but also because of the difficult problems that needs to be solved. CLIC problems are shown in the bullet list underneath and will be explained, from [2, p.21];

- Achieve a main Linear Accelerator (Linac) gradient of 100 MV/m.
- Generation and preservation of the ultra-low emittance of the beam to achieve necessary luminosity.
- Generation and extraction of energy from a drive beam to the main beam.
- Ability to protect the machine (This report will not go through design for protection).

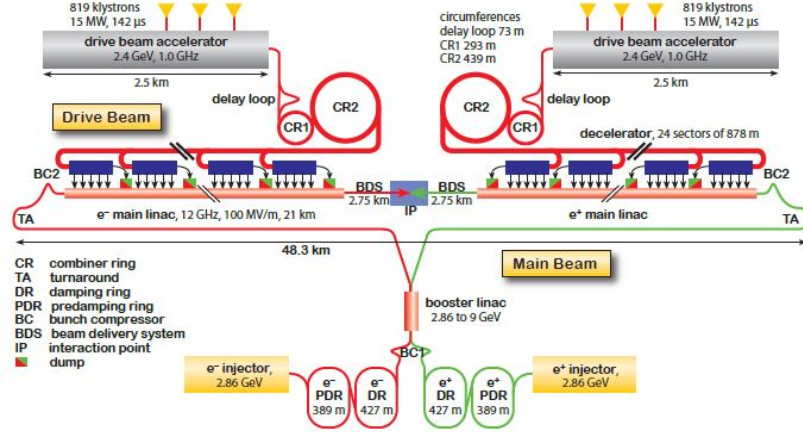


Figure 2.2: Overview of the CLIC layout at 3 TeV. This picture shows the whole complex. At the top we can see the drive beam linear accelerators that will start the drive beam process. This beam then enters a delay loop and two combiner rings to reach the necessary pulse behaviour. This drive beam then comes to the PETS structures which will transfer energy to the main beam. In the bottom we have the electron and positron injectors together with their Linac structures. These two beams then go through bunch compressors to reach the necessary behaviour before reaching the turnarounds where the main Linac starts. In the middle of the picture we can see the IP where the electrons, positrons will collide with the help of final crab cavities that steer the particles toward collision. From [2, p.19]

To understand why the machine needs to preserve the ultra-low emittance that the dampening rings will achieve, we need to understand how luminosity depends on different machine parameters. Luminosity being a parameter describing how many particles there is and therefore describing how many that can be collided. Equation 2.1 shows how the luminosity can be written for a linear collider. From [18]

$$L = H_D \frac{N^2}{\sigma_x \sigma_y} n_b f_r \Rightarrow L = H_D \frac{N^2}{\sigma_x \sigma_y} \frac{P_b}{E_b} \quad (2.1)$$

Here  $H_d$  is a correction factor,  $N$  is the number of particles per bunch,  $\sigma_x$  and  $\sigma_y$  is the r.m.s (root mean square) beam size in horizontal/vertical direction respectively at the point of interaction,  $n_b$  is the number of bunches per pulse and  $f_r$  is the repetition rate of the linac structure. The two last values  $n_b$  and  $f_r$  can be rewritten to show the energy of the beam instead. This can be more interesting since one usually compares energy in colliders. Then  $P_b$  shows the beam power and  $E_b$  the beam energy.

In order to reach the necessary luminosity it can see from equation 2.1 that the beam size which is proportional to the emittance needs to be as small as possible. Equation 2.2 shows how the emittance relate to the beam size.  $\gamma$  is the Lorentz factor and tells how relativistic a particle is.

$$\sigma_{x,y} = \sqrt{\frac{\epsilon_{x,y} \beta_{x,y}}{\gamma}} \quad (2.2)$$

Due to acceleration the emittance will not be conserved. One could think that there would be an option to change and lower the beta function to get smaller beam size but unfortunately lower limits already exist on the beta function. These limits comes from the optics and design of the beam delivery system. So the only option to get the necessary luminosity is to create an ultra-low emittance, see [1, p 11-13].

Why it is hard to achieve a high accelerating gradient inside the structure of CLIC is due to the so called breakdowns. Therefore facilities and test stands have been constructed to understand and develop technology for breakdown studies, for projects such as CLIC and Free electron lasers (FELs). Breakdowns can not only ruin the structure itself, it can also affect the beam in negative ways. Both the transversal and the longitudinal beam momentum can be affected. Going back to equation 2.1 we can see that effects on the beam size directly affect the luminosity. Since

CLIC requires a very low emittance beam to be able to deliver high luminosity to experiments, this effect cannot be allowed to be large, [16]. An important contributor to these studies is the CTF3 collaboration group. They have been studying this phenomena inside accelerating structures since 2005 [3]. The group has also constructed different test stands called XBox to further understand this problem.

### 2.1.2 CTF3

One objective the CTF3 collaboration had was to construct a 30 GHz test facility where test of high gradient structures were conducted. This test stand was in operation from 2005[10]. The first major problem was to reach the nominal gradient of CLIC at 150MV/m where a loaded gradient is set to 100MV/m. As mentioned before a loaded gradient of 100 MV/m is the aim for the CLIC project and this with a Breakdown Rate (BDR) of  $10^{-7}$ , which is the hardest part to achieve. BDR is the derivative of how many electric discharges that occur in the structure with respect to the number of pulses sent. Together with higher gradient comes higher BDR and vice versa. CLIC design group have after optimization decided that 100 MV/m is a good value for optimal cost and efficiency. For further improving and testing the CLIC feasibility the TBTS was constructed. Great success of TBTS was to achieve the two-beam acceleration scheme, but since the TBTS was constructed with great beam diagnostic tools it could be used for RF breakdown studies as well. TBTS is together with the CTF3 facility going out of commission in 2016. Options to reuse equipments exist, for example they plan to use klystrons to power the accelerating structures instead of using the two beam scheme.

### 2.1.3 Cavities

A cavity is an accelerating structure used to increasing a beam's energy, see 2.3 for a picture over a cavity in this case the T24OPEN, used in this thesis. This is done by generation of an external electric field. This electric field will flow between different cells and will have a maximum value in between, at a position called iris. Iris is the smallest transversally part of the cavity. There are different types and forms on cavities but the concept is to have cylindrical cells. In each cell particles will gain energy by arriving inside at correct phase compared to the electric field. Next cell will have de-accelerating field, but since the field changes direction when the particles arrives at next cell the particle is further accelerated.

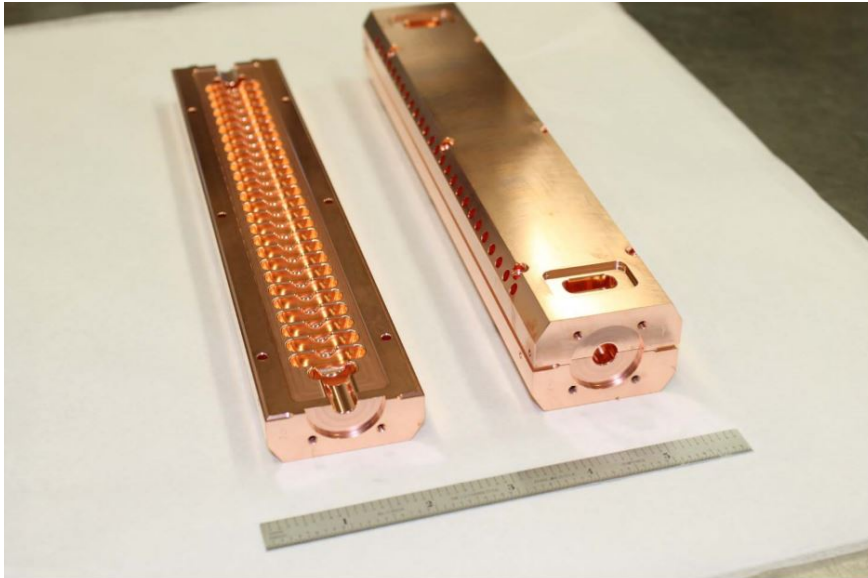


Figure 2.3: Picture over two halves together and one half open of the T24OPEN cavity. From [19]

### 2.1.3.1 T24OPEN Cavity

This thesis work has been done while the T24OPEN cavity of the X-Box2 was used. The T24OPEN is a cavity constructed from two halves and then put together. This is called an open structure and is where the name comes from. Earlier structures have been a stack of single discs which when stacked together and brazed form the cells of the accelerating structure. Now both halves can be directly brazed reducing the number of parts needing to be brazed. Brazing is an approach that can create unwanted RF flows inside the structure. This since it can create sharp edges where the field is higher, which will ruin the acceleration of particles and also make the copper soften due to the high temperature. The lower amount of parts will also reduce the cost of production. Table 2.4 shows the specification of the cavity.

Loaded gradient* [MV/m]	100
Working frequency [GHz]	11.994
Phase advance per cell	$2\pi/3$
Active structure length [mm]	217
Input/output radii [mm]	3.15/2.35
Input/output iris thickness [mm]	1.67/1.00
Q factor [Cu]	7112/7445
Group velocity [%c]	1.99/1.06
Shunt impedance [M $\Omega$ /m]	107/137
Peak input power [MW]	60.9
Filling time [ns]	49.5
Maximum E-field [MV/m]	313
Maximum modified Poynting vector[MW/mm <sup>2</sup> ]	7.09
Maximum pluse heating temperature rise [K]	35

Figure 2.4: Specifications of the T24OPEN cavity from SLAC. From [19]

For use in breakdown positioning the important specifications are:

- Working Frequency: To be able to determine the velocity of RF signals inside the waveguide system.
- Phase advance per cell: The phase of the pulse will be necessary in order to see that the structure works as intended and can be used to further improve the accuracy of positioning.
- Active structure length: Used to calculate the time it takes for the pulse to go through the structure, see Filling time.
- Group velocity: Most important is to know the velocity of the RF signals inside the cavity. This will be used to accurately calculate the time of the different signals to travel through the cavity and be measured. This can then be used to see in which structure cell the breakdown occurred.
- Filling time: Can be calculated by using the group velocity together with the length of the active structure.

### 2.1.4 Conditioning

New cavities are put under RF tests to gradually bring the structure to the nominal parameters with respect to gradient, pulse length and the BDR. This is said to make the cavity condition. A typical conditioning process can be seen in figure 2.5. By sending in a pulse with low power and short length the conditioning starts. In the beginning before conditioning has started a cavity can have a BDR in the order of  $10^{-3}$  per pulse. This is much higher than the goal of  $10^{-7}$ . If higher power, meaning higher gradient had been used immediately, the cavity would quickly be destroyed. By having this process starting weak and gradually increasing the power and pulse length, the cavity will hold a stable BDR. Going to fast will as been said break the cavity while too slow would take time. We can see in the figure that in the end of the process the BDR drops down. This since both power and length is enough and the cavity can therefore be called conditioned. Most interesting with the conditioning plot is how the BDR seems to de-

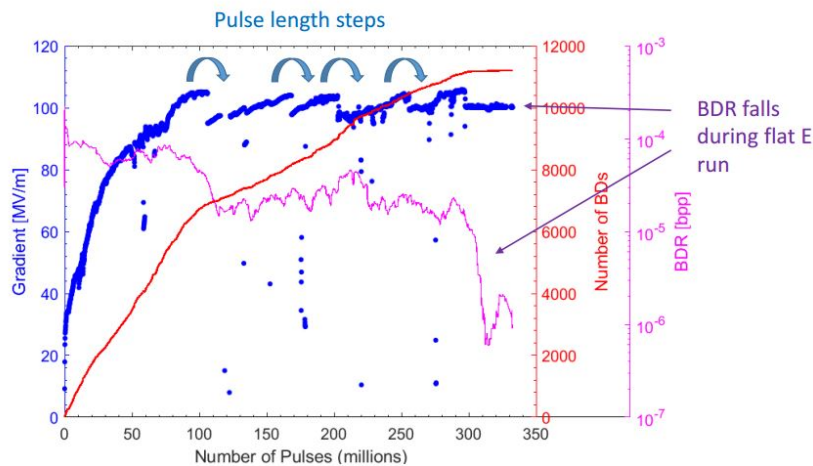


Figure 2.5: Plot over data for a typical conditioning process for CLIC cavities. Blue dotted line shows the gradient change over total number of pulses. Small jumps happens when the pulse length is changed to further condition the cavity. Red line shows the total number of breakdowns over the total number of pulses. Magenta colored line shows the derivative of the red line called BDR. As we can see the BDR slowly decreases when optimizing the conditioning process to not damage the structure. From [14]

pend on the number of pulses instead of pulse power. This makes the condition process slow since it run with 50 Hz.

It is important to try different cavity types to understand if the process of creation of the cavity can have any impact in how fast and well the cavity goes through the conditioning process.

The previous Crab cavity helps the particle beam collide in a limited and controlled area right before the IP



of the CLIC facility. A couple of cavities have been tested, as can be seen from figure 2.6, and the conditioning process always look the same, even despite different conditioning approaches [13]. Using the same ways of measuring but now with perspective of the total number of breakdowns or accumulated breakdowns versus the scaled gradients the plots shows no form of correlation, see figure 2.7. This means that conditioning depends on the total number of pulses and not the number of breakdowns, meaning that looking on number of pulses and correlating this to the conditioning process, will help when optimizing the conditioning of high gradient structures based on this experimental evidence, see [13] for further information.

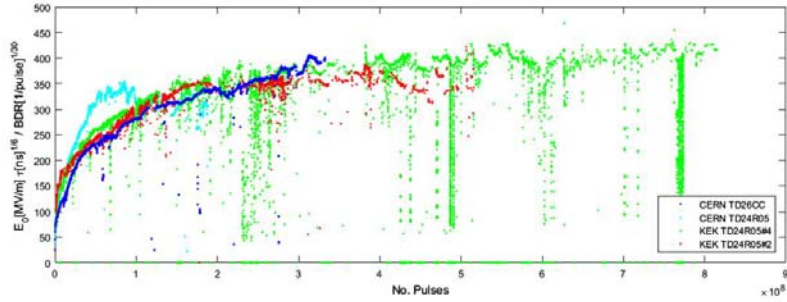


Figure 2.6: A comparison of different cavities and their specific conditioning process. X-axis is the number of pulses while the Y-axis have the scaled gradient. From [13]

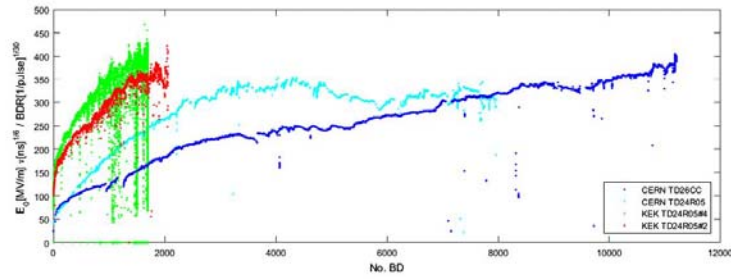


Figure 2.7: A comparison of different cavities and their specific conditioning process. X-axis is the number accumulated breakdowns while the Y-axis have the scaled gradient. From [13]

### 2.1.5 X-Box

XBox is at this moment a project consisting of two test stands created for the purpose of testing multiple CLIC structures. This to both improve and understand the physics behind RF breakdown together with the process of conditioning. This process however is very slow, takes some months to do. This due to the low repetition rate (50 Hz) of the pulses in the Xbox test stand. Since there is a need for more cavities to be tested more test stands are being built.

The subsections beneath will give a brief description of the two X-band stand now in work [9] see figure 2.8.


 Xbox-1 OPERATIONAL	 Xbox-2 OPERATIONAL	 Xbox-3 COMMISSIONING February 2016
CPI 50MW 1.5us klystron Scandinova Modulator Rep Rate 50Hz Beam test capabilities	CPI 50MW 1.5us klystron Scandinova Modulator Rep Rate 50Hz	4x Toshiba 6MW 5us klystron 4x Scandinova Modulators <b>Rep Rate 400Hz</b>
<b>Previous tests:</b> 2013 TD24R05 (CTF2) 2013 TD26CC-N1 (CTF2) 2014-15 T24 (Dogleg)	<b>Previous tests:</b> 2014-15 CLIC Crab Cavity	<b>Medium power tests (Xbox-3A):</b> 2015 3D-printed Ti waveguide 2015 X-band RF valve
<b>Ongoing test:</b> Aug2015- TD26CC-N1 (Dogleg)	<b>Ongoing test:</b> Sep2015- T24OPEN	<b>Major increase in testing capacity!</b>

Figure 2.8: Figure over the three different X-Box setups. Xbox1 is to the far left and have had multiple cavities tested with similar results. Xbox2 commissioned September 2015 and are with tests on CLIC crab cavity and now the T24OPEN is put in. Xbox3 says to be commissioned in February of 2016 but is of yet in condition to test cavities. From [14]

### 2.1.5.1 X-Box 1

X-Box1 was as implied the first X-band RF test stand to be constructed. When constructed this was the only place except CTF3 where one could use the required power and pulse length on a 12 GHz RF pulse. Similar X-band tests, meaning tests in the frequency range of 8-12 GHz, have been done in both Stanford National Accelerator Laboratory (SLAC) USA and The High Energy Accelerator Research Organization, Tsukuba, Japan (KEK) Japan. Since CLIC uses 12 GHz and not 11.4 GHz as tested at SLAC, many of the components had to be redesigned for this specific usage [8].

### 2.1.5.2 X-Box 2

Due to an increasing number of cavities to be tested and limited capacity of the xbox1. CERN builds an improved copy of the X-Box1 test stand (X-Box2). This new test stand differs from its predecessor by having a newer more developed Low Level Radio Frequency (LLRF) system together with a more enhanced pulse compressor system [8]. X-Box2 has during the last couple of months been running with a relatively low power because of trouble with radiation. This problem will most likely be fixed in the summer of 2016 when an extra layer of concrete will be put on top of the bunker roof.

### 2.1.5.3 UCXS

The Uppsala/CLIC X-band spectrometer (UCXS) situated after the cavity in the X-Box2 test stand was made in order to receive more information regarding dark currents and breakdown currents.

UCXS was installed during the same time as the crab cavity in 2014, more details of the setup and usage in section 3.2. UCXS includes a collimator, screen chamber with a fluorescent screen, downstream faraday cup and a dipole magnet, see figure 2.9. The dipole has not been used until just recently with very little result. More about the images will be found in chapter 4 section 4.5.1.



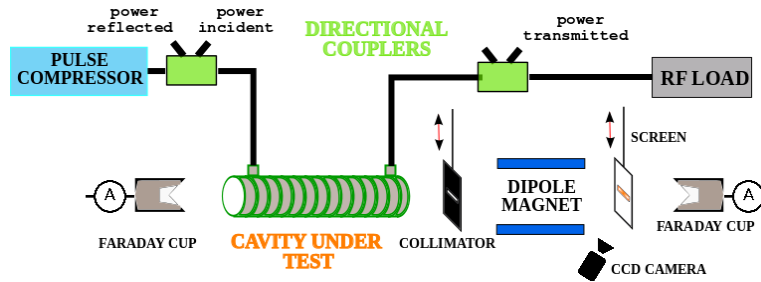


Figure 2.9: Schematic over the setup inside the bunker with a more thoroughly illustration of the UCXS. From [6]

## 2.2 Vacuum Discharges

Electrical discharges have been seen and known for a very long time. Still when it comes to discharges in vacuum theorists and experimentalists are having wide discussion about this special phenomena. When going into vacuum regions, models that try to describe how discharges appear have one thing in common, that is to ignore the Paschen's law of breakdown voltage. This means that the gas pressure is low enough to totally neglect interactions between gas particles [11]. Common understanding is that the vacuum discharge is initiated by a field emitted electrons from the surface under the presence of external electric field. Field emission theory was formulated by Fowler and Nordheim, see [21]. These two derived an equation that put current density as a function of electric field. Field emission theory is a quantum mechanical effect of tunnelling and electrons can be emitted when high enough electromagnetic field exist to go through the barrier. These equations are rough approximations of reality and more and better ways of approximating the problem are theorised. Emitters are most material of the structure itself or of impure particles such as dust. The areas will have temporary electric fields, with gradients up to 10 GV/m. Breakdown is an electrical discharge which appears in high electrical field places. Before a breakdown happens there can be seen a dark current. This is a current coming from accelerated electrons that is emitted from emitter sites under high electromagnetic field. If one of these emitters have a high temperature emitted electrons can be further accelerated if in correct phase. When enough charged particles are gathered an arc will be formed and become self-sustained and free charged particles will once again be accelerated. This stronger current is called a breakdown. Physics to understand these breakdowns in vacuum is not yet fully developed in the same way as when discharges appears in air.

There are two types of experiments used for understanding how breakdowns appear in vacuum: using a pulsed DC signal and the use of RF. RF signals is what accelerators use in order to reach the necessary gradient. The repetition rate used at current experimental setup is only 50 Hz. By using pulsed DC instead this repetition rate can be increased to kHz and therefore data can be gathered much faster and samples can be easily changed. DC systems are usually much smaller and cheaper as well with a longer pulse length, which makes a DC system attractive. The advantage of using RF is that studies of distributions inside the cavity and field effects can be directly studied, which cannot be done with a DC setup. DC and RF breakdowns have been studied separately but have a lot in common. Therefore both can be studied under different conditions and still have results for both cases [12]. CERN have started studies from both directions in order for future high energy physics research to evolve to the next stage.

# Chapter 3

## Instrumental Set-Up

This chapter gives a detailed view and explanation of the experimental setup X-Box2 and the UCXS instrument used together with the setup. From section 2.1.5 a small background has already been given to and the X-Box studies and why this work is important.

### 3.1 X-Box2

The main reason behind building the new test stand X-Box2 was to increase the possibility to test new structures. The schematic of X-Box2 can be seen below in figure 3.1. The test stand consists of a modulator and klystron that

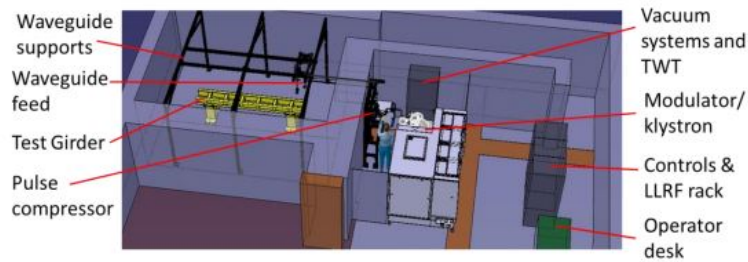


Figure 3.1: Overview of the test stand X-Box2. From [8, p.41]

will give the needed 50 MW power to the RF pulse. Formation of the pulse is done by the control and LLRF rack situated right before the entrance to the bunker. The pulse is then sent into a waveguide going through a pulse compressor, and is then received inside the bunker by the cavity.

The LLRF system creates a phase modulated pulse. In order for the system to be able to detect breakdowns and fast changes in the RF signals, the required time resolution has to be down to one nanosecond. This can then be used to detect changes and backwards calculate with enough precision in which cell of the cavity a breakdown has occurred. The system have a sample rate of 1.6 G sample/s with a 12 bit resolution. Klystron and modulator are the same as for X-Box1. As mentioned before, the klystrons are based on the klystrons at SLAC and KEK but have a scaled frequency, from 11.4 GHz to 12 GHz with 50 MW peak power. The modulator used for X-Box needs to give a voltage of 410 kV together with a current of 310 A. Modulators of this kind are hard to produce and since CERN wanted high flexibility a solid state modulator was necessary. This meant that only one manufacturer in the world was able to give this to CERN, namely Scandinova [8].

A pulse formed by the klystron travels to the pulse compressor SLED-1. Here the pulse will increase in power with the cost of pulse length. More can be found in [8]. Important to know is that X-Box2 uses an upgraded pulse compressor that can create less unwanted modes by using adiabatic tapers at each end. There also exist mode converters to further decrease the losses of RF power.

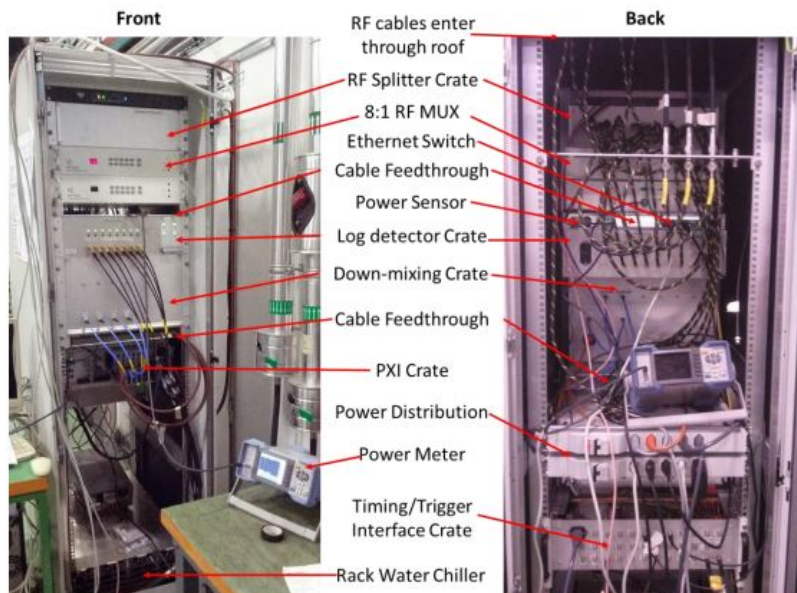


Figure 3.2: Photo taken of the LLRF and control rack used for X-Box2. From [8, p.60]

From the pulse compressor the pulse travels through the waveguide components into the bunker. Since the frequency of the pulse is 12 GHz these waveguides are very small, only a few centimetres in both height and width. This is a reason to why high frequency accelerating structures are very attractive. With smaller waveguide systems less space is required often making the whole structure cheaper. The cost is not always true since there already exists larger waveguide systems throughout CERN that are scrapped or just out of order and can be reused if ever needed. Tolerance however have to be higher since there is an increased risk for discharges. For X-Box2 there is also a new set of high power RF components that is tried out. These are vacuum ports and valves used to keep the vacuum at a low level in between two waveguides when vented and still be able to cancel reflections that can be introduced when systems need to be fused together. Figure 3.3 shows how the setup inside the bunker looks like.

When the pulse reaches the inside of the bunker it comes to a directional coupler. A directional coupler is sort of an interface between the vacuum system and the LLRF system giving the possibility to read the signal and then use it for the purpose of understanding what happens inside the structure. In figure 3.3 we can see two 60 dB directional couplers situated in the beginning of the structure and one at the end. The first coupler receive input and reflected signals, while the coupler after receives a transmitted signal which tells how much of the signal that has gone through the structure. Due to losses of power when a breakdown occurs the RF load at the end will become unmatched giving a reflection back through the structure. This is easily distinguishable when checking the RF pulse data saved from the LLRF rack. More about the signals can be read in chapter 4.

After the directional couplers the pulse goes into the on test structure. In figure 3.3 the cavity is the Crab Cavity, but from September 2015 until now the cavity is T24Open. On both side of the cavity there is an upstream and downstream ion gauge readout and faraday cup. Ion gauges will monitor the neighbouring pressure levels to ensure that a high vacuum exists while the faraday cups will measure any dark current that comes out from the cavity. As can be seen in the figure 3.3 the downstream faraday cup is blocked by the UCXS and will currently only receive small currents. This is mainly because of the collimator blocking a huge part of the current that can be received by the faraday cup.

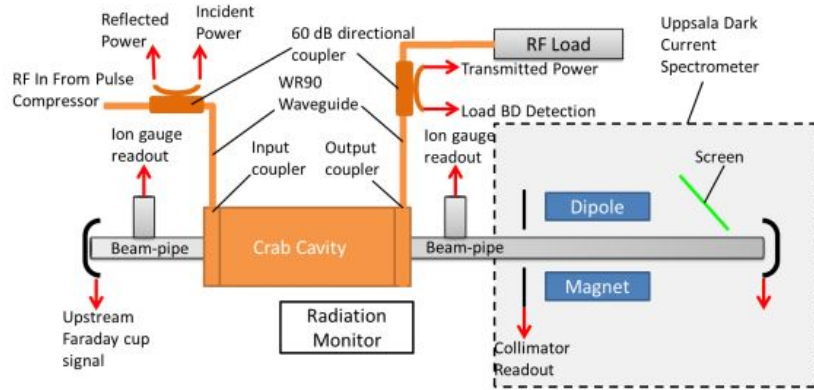


Figure 3.3: Scheme over the diagnostic part of the X-Box2 test stand. Upstream the cavity (Crab cavity in figure) is situated while downstream we can see the UCXS. From [8, p.144]

### 3.2 Uppsala spectrometer

This spectrometer can be seen in figure 3.4. It is situated at the end of the test stand downstream from the cavity. In the figure one can see the cavity on the far left side with waveguides feeding it with RF signals. In the beginning

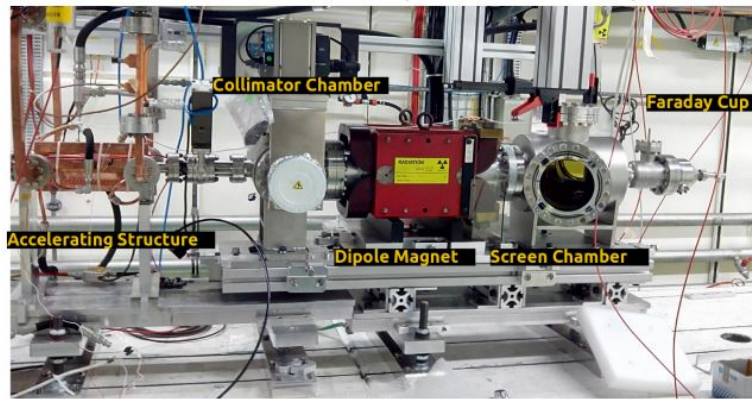


Figure 3.4: Picture of the UCXS situated at the end of the test stand. From [6]

of the spectrometer there is a tungsten collimator with two different types of openings. There is a slit with the measurements  $10 \times 0.5$  mm and a pinhole with the diameter of 0.5 mm. To use both openings a motor was installed that can move the collimator remotely from Uppsala. Inside the screen chamber there is a fluorescent screen with the measurements  $100 \times 50 \times 0.5$  mm. The screen is situated at a 30 degrees angle from the beam's axis and the photons that comes from the screen after interaction are then reflected by a mirror with 90 degrees angle onto a 2M pixel CCD camera. Pulses have a repetition rate of 50 Hz and the camera has to have at least 50 frames per second acquisition. To be able to get a good image a stepper motor was installed for the focusing of the camera and this can be remotely moved. This motor can focus the image in small steps, for the camera it is down to ten microns. The screen frame can also be moved with the help of a stepper motor. This is to have the possibility of changing the distance from the beam axis and also take the screen away if ever necessary. [4]

# Chapter 4

## Data Analysis

In this chapter the data analysis from the experiments done with UCXS spectrometer at X-Box2 is presented. Data used is collected at CERN and Uppsala and given in the form necessary for analysis. How the data then is used and processed will be explained in the sections of this chapter. Analysis is done in MATLAB and the source code is given in Appendix B.

### 4.1 Data format

There are two different system that collect information. The LLRF system that collects signals and the UCXS system that uses the same triggers as the LLRF for when data will be saved. Both systems run under LabView software.

The LLRF system saves 16 different signals from each RF pulse with a maximum of 50 Hz (20 ms). These are RF-signals processed by Q/I detectors or log detectors, Faraday cup signals processed by ADC converters and a collimator signal now swapped to a BLM. These signals can be seen in table 4.1.

Table 4.1: Table over signals received

Signal	Sample rate
Klystron Output Amplitude (PKI)	1.6 GHz (0.625 ns)
Klystron Output Phase (PKI)	1.6 GHz (0.625 ns)
Structure Input Amplitude (PSI)	1.6 GHz (0.625 ns)
Structure Input Phase (PSI)	1.6 GHz (0.625 ns)
Structure Reflected Amplitude (PSR)	1.6 GHz (0.625 ns)
Structure Reflected Phase (PSR)	1.6 GHz (0.625 ns)
Structure Transmitted Amplitude (PEI)	1.6 GHz (0.625 ns)
Structure Transmitted Phase (PEI)	1.6 GHz (0.625 ns)
Klystron Output Log Amplitude (PKI)	250 MHz (4 ns)
Faraday-cup downstream (DC-Down)	250 MHz (4 ns)
Structure Reflected Log Amplitude (PSR)	250 MHz (4 ns)
Collimator (Now BLM)	250 MHz (4 ns)
Klystron Reflected Log Amplitude (PKR)	250 MHz (4 ns)
Klystron Input Log Amplitude (Kly IN)	250 MHz (4 ns)
Load Reflected Log Amplitude (PER)	250 MHz (4 ns)
Faraday-cup Upstream (DC-Up)	250 MHz (4 ns)

Events are logged and saved to hard drives automatically each minute. When a breakdown occurs, the faraday cup or the log signals exceeds a certain threshold, the current event and the two preceding events will be saved. After a breakdown occurs the system will stop for a few seconds to then resume the conditioning process and data collection. Figure 4.1 shows how the signals look for a breakdown event.

The UCXS system takes images at a 50 Hz rate, each 20 ms. When a breakdown occurs the LLRF system is

triggered and signals the UCXS system and the images can be saved. Together with image over breakdown event, three preceding and one proceeding image is saved to be used as background subtraction. The UCXS system will also receive a copy of the breakdown event from the LLRF system for collection of data. The signal named colli-

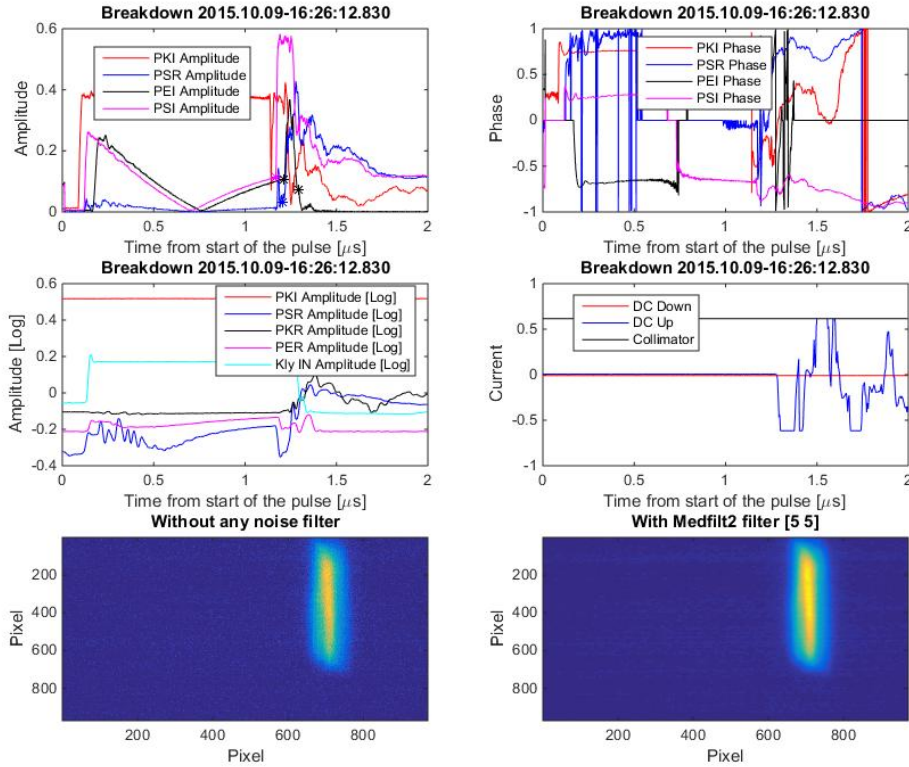


Figure 4.1: Plot over the signals during a typical breakdown event (Breakdown event name given as title to each plot, where the name used is connected to time of occurrence). Top left corner is the amplitude of the RF-signals. Top right corner have phase signals in the scale of -1 to 1, where 1 is set to be 180 degrees making -1 to 1 being 360 degrees. Middle left is the signals amplitude in logarithmic scale used for breakdown flagging. Middle right is the three last signals where only the upstream faraday-cup signal is used. Bottom left is an image over the event where bottom right is the same image with a median filter applied, both use a color map to easier distinguish spots of photons

mator has not been used since installed. This signal was supposed to be used like a faraday cup signal measuring charge over a 50 ohm resistance that is situated at the collimator. This signal worked but had very fluctuating signals. Decision to remove it was made, but it will be used again whenever better adjustment to the system is done. Now since February 2016 this signal has been changed to be used for a **BML!** (**BML!**). This signal is used to gather data from the newly installed optical fibre which interacts with radiation from the cavity. These fibres work as cherenkov radiators where each end will be coupled to photo sensors. So when particles cross the optical fibre, cherenkov photons will start to propagate through the fibre. Radiation have previously been measured from radiation monitors inside, right next to the setup and outside the bunker.



## 4.2 Data Conversion

To be able to analyse data in MATLAB from X-Box2 multiple conversions had to be done.

Data coming from X-Box2 is in the form of TDMS. Using a subroutine from Mathworks a conversion of TDMS format to .mat was done. This data includes everything that exist in the TDMS files in the form of structures in MATLAB. By using this conversion it is easy to form a MATLAB script that can have a handle to necessary data.

Data from X-Box2 is also received by Uppsala in the same format but is saved together with images from the UCXS. These images are necessary for analysis and they are therefore necessary to implement together with the RF signal data. By gathering data from Uppsala in the form of .TXT and images in .PNG, MATLAB functions to combine data from X-Box2 and Uppsala could be done. This makes final data after 4 steps of conversion include every thing necessary to have a complete analysis of breakdown events inside X-Box2.

Each breakdown event can be single handedly measured and plotted in the MATLAB code written. This is done by manually choosing the interesting event name (seen as title in both figure 4.1 and figure 4.2) and look through the plot. To see changes between interesting events a code to compare data plots from two events was written, see figure 4.2. Knowledge about the amplitude and phase is usually what is interesting to compare, therefore the plots only show these signals together with an image. This is both to increase the resolution of the figure as well as making the code as easy as possible to change and understand. From experience one will always check the amplitude of the RF pulses to see how a specific breakdown differs from another, in case of a big difference the pulse data may be analysed.

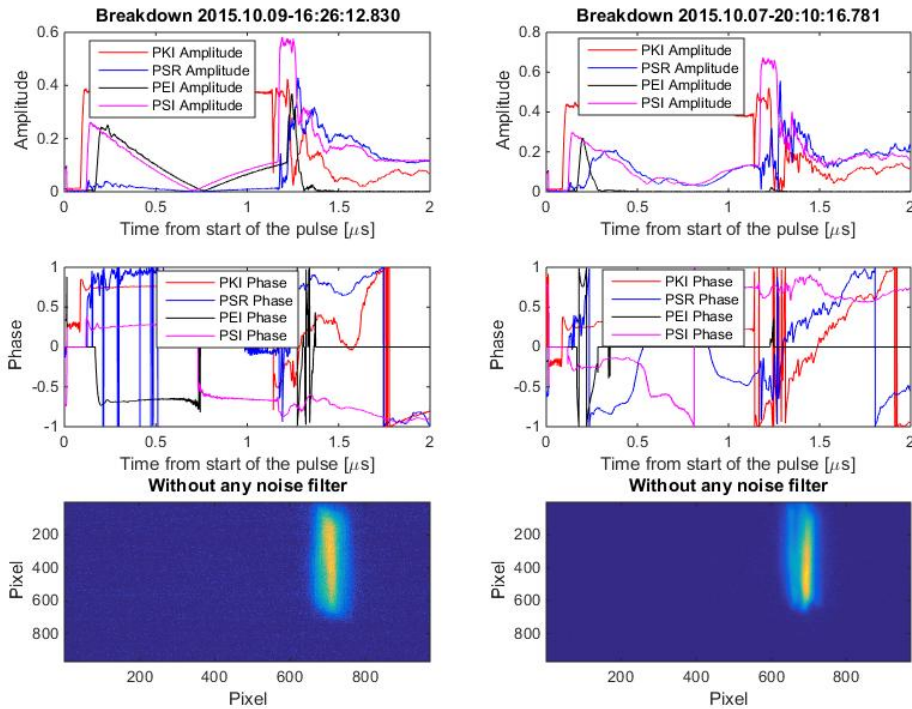


Figure 4.2: Plot to be able to compare two different events. Used for troubleshooting and finding why some events are hard to analyse.

### 4.3 Breakdown Positioning

When a breakdown occurs information will be gathered due to signals breaching the thresholds. Timing measurements from the different signals can be done based on when they have reached the data logging system. This gives an identification to where inside the cavity a breakdown has occurred. It is possible to measure the speed that the RF signals travels with through the whole structure, including the waveguide system. By knowing the speed of the signals a difference between them can be related to a distance. By forming different methods to try and describe and compare the signals it is possible to say where the position of a breakdown is located and compare the result of each method. This gives further information to where in a cavity breakdowns appear, if they are earlier or later in the structure. Signals used for the methods in this thesis are: Structure reflected amplitude (PSR), Structure input amplitude (PSI), Structure transmitted amplitude (PEI), Faraday-cup upstream (DC-Up), Structure reflected phase (PSR) and Structure transmitted phase (PEI). The three amplitude signals together with the faraday-cup signal have a time distribution that shows the time of breakdown for each one of them, this can be seen in figures 1, 2, 3, 4 in appendix A. These distributions are over all events analysed and shows how much they can change. By calculating the breakdown position and then making a distribution for all events, an analysis can be done.

It is also interesting to see if the methods give the same results or not. Therefore distributions over the differences can be done and analysed.

### 4.4 Longitudinal Methods

Different methods on how and what information we can get out of the RF signals will be shown in this section. Data used for these longitudinal methods comes only from September 2016 - December 2016. The methods used and analysed in this thesis are:

- Edge Method
- Correlation Method
- Faraday-Cup Method

All methods use one or more amplitude signals. For this reason it is necessary to have a higher accuracy on these signals. For the Faraday-cup signals two different exists. The Up-stream signal is measured at the faraday cup before the cavity while the downstream faraday cup is now blocked by the UCXS, so only the upstream can be used. See section 3.1 figure 3.3.

#### 4.4.1 Edge Method

The edge method uses two of the 16 signals from the LLRF. Here the falling edge (80% of the peak value) of the transmitted and the rising edge (20% of the bottom value) of the reflected signal is going to be used. The reflected signal will be received by the system with a delay due to the travel distance. From the threshold signals we know when a breakdown has occurred. Using this information the time delay between the reflected and the transmitted can be calculated. Figure 4.3 shows at which side the signals will be detected. When receiving the signal data it is

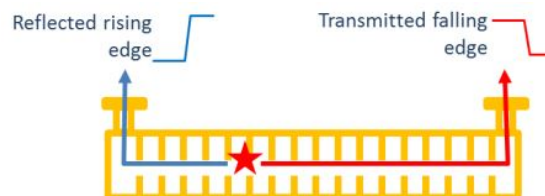


Figure 4.3: Time calculation illustration for the Edge method. From [8, p.155].

necessary to align both signals to each other. The reflected signal is received by the upstream directional coupler meaning it first needs to enter the cavity and then go back. The transmitted signal is received by the downstream



coupler and it only needs to go through the structure. This means all together that by knowing the filling time  $t_{fill}$  see 2.4, it is possible to align the signals and then calculate the difference between both signals. The transmitted signal  $t_{tf}$  has an extra time from the cavity to the couplers which add 6.2 ns while this time for the reflected signal  $t_{ref}$  is 6.56 ns, giving a total extra time  $t_{ex}$  without the cavity time of 0.36 ns. This difference can then together with the knowledge of group velocity  $v_g$  and length of the cells  $l_{cell}$  see 2.4 inside the cavity be translated to position or cell number  $Nr_{cell}$ , see equation 4.1.

$$t_d = \left( \frac{t_{fill} + t_{ref} - t_{tf} + t_{ex}}{2} \right), Nr_{cell} = \frac{v_g * t_d}{l_{cell}} \quad (4.1)$$

Figure 4.4 shows a typical signal. Star marked positions in the top left plot show the calculated signals timings when using the edge method. As can be seen in the figure the reflected signal (blue) and the transmitted signal (black) usually lie close to each other. When calculating the edge method a script is used that removes the background. The transmitted signal is negative due to background subtraction and transmission being less during a breakdown. This subtraction is done by using two signals from one (20 ms) and two (40 ms) events before when no breakdown occurred. By doing this it gives a more reliable result for the edge method. What also was necessary to do was a short correlation code that checked if the three different pulses had the same time scale. This means that the system can, if it becomes delayed by a few samples both ways, be corrected. So to be able to subtract the background the correlation needs to be as good as possible for the signals right before the signal enters the cavity, which time lies around  $1.16 \mu s$ . Some events have been found where the reflected signal happens much earlier (within the first 500 ns) and these events are discarded due to unreliability. Signals can however come from an early breakdown happening in the waveguide system and even in the pulse compressor, see figure 4.5.

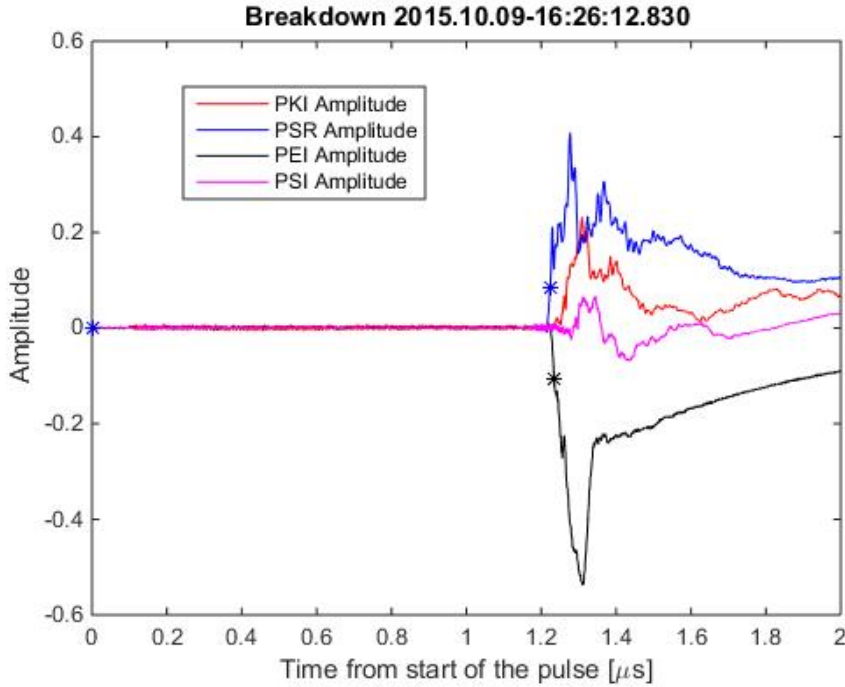


Figure 4.4: Signal when calculating edge method time. Stars on the RF signals show what positions is chosen from the algorithm

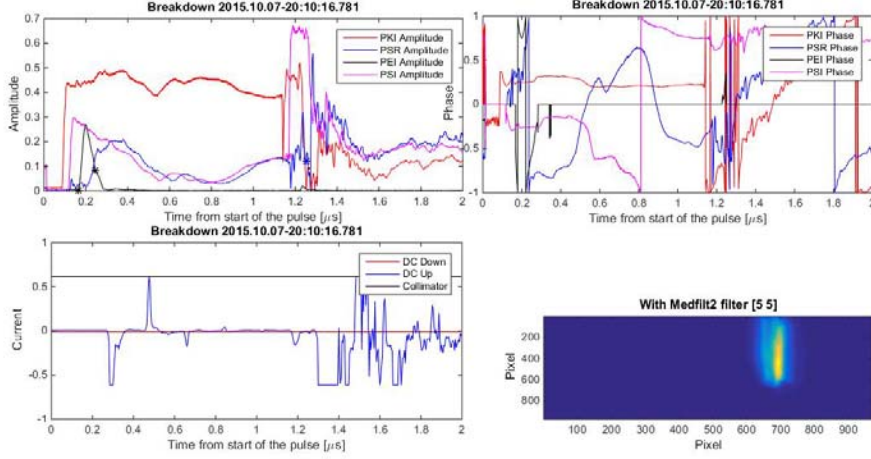


Figure 4.5: Breakdown event with a very early breakdown signal

#### 4.4.2 Correlation Method

The correlation method uses the structure input signal falling edge (70% of the peak value) and the best correlated reflected signal to calculate the breakdown position. It is necessary to first find an edge where calculation can start from. During a breakdown we observe multiple reflections of the incoming and reflected signal. The shift in time between these reflections indicated how deep into the structure the breakdown occurred. Since the signals usually are a lot stronger at the maximum point of power (where the amplitude is biggest) this operation usually starts at the tail of the signal to better find a replication. A correlation search is then applied to the reflected signal at the chosen position with a range from  $0 \rightarrow 2 * t_{fill}$ , since the maximum time difference can only become the length of the structure. The correlation algorithm uses MATLAB's built in function `corr`, which calculates the linear dependence of the values, see equation 4.2 how it is calculated. After calculating the cross-correlation between the two signals, the maximum of the cross-correlation indicates the point in time where these signals are best aligned to one another. Here A and B is the different values,  $\mu_A$  and  $\sigma_A$  is the mean and standard deviation of A or B, N is the total number of values calculated.

$$p(A, B) = \frac{1}{N-1} \sum_{i=1}^N \left( \frac{A_i - \mu_A}{\sigma_A} \right) \left( \frac{B_i - \mu_B}{\sigma_B} \right) \quad (4.2)$$

Figure 4.7 shows points chosen for a typical correlation method result. Alignment is easy to do since the signals are measured from the same coupler with the only difference that the reflected signal goes into the cavity and back, therefore the delayed time needs to be divided by two. No background subtraction is done for the correlation calculation due to making start location unreliable.

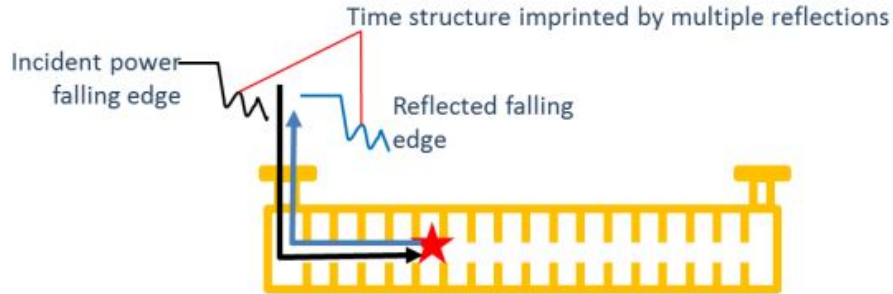


Figure 4.6: Time calculation illustration for the Correlation method. From [8, p.156].

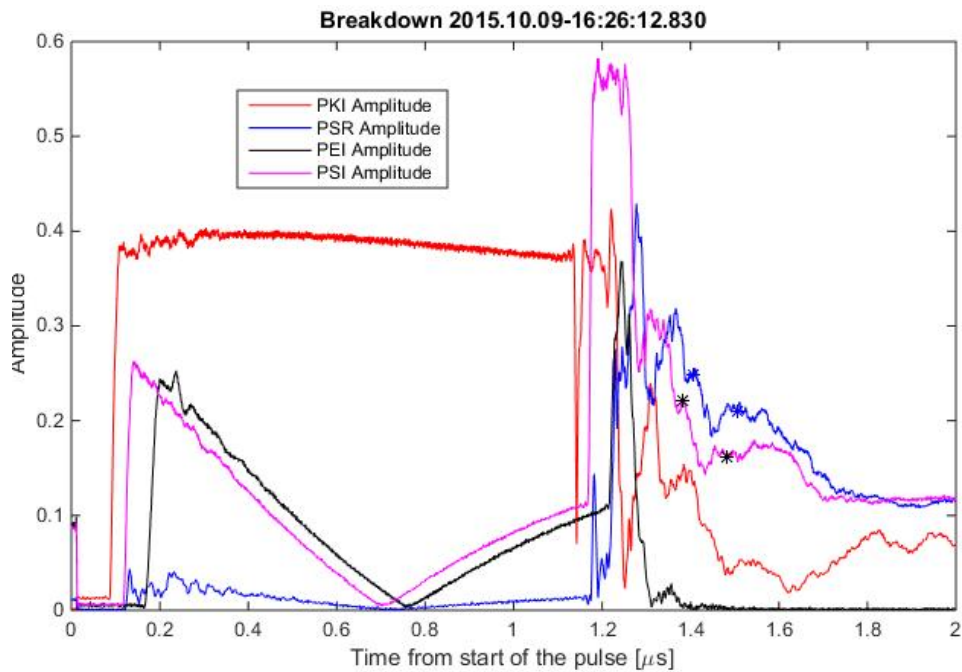


Figure 4.7: Signal when calculating correlation method time. Stars on the RF signals show what positions is chosen from the algorithm, black points for the input signal start point and end point and the blue points are start and final reflecting signal positions.

#### 4.4.3 Faraday-Cup Method [FC-Method]

A new method of finding the breakdown positions was what in this thesis is described as the Faraday-cup method (method idea from [17]). This method uses the signal from the faraday cup situated upstream from the cavity versus the falling edge (90% of peak value) of the transmitted signal. When a breakdown occurs a big spike in the faraday cup signal can be seen, see example figure 4.8. This signal is saturated and does not give a full description of how high the current is. However the signal can be used to determine when a breakdown occurs but with an inaccurate timing. This timing is not fully trustworthy since no alignment can be done. It is also important to note that the FC signal has a sample rate that differs from the transmitted signal. To be able to use both signals together an interpolation of the FC signal was done making the distance between each point the same as for the

transmitted signal. This made it possible to make a distribution for the method with a better accuracy, but still inaccurate since the alignment still cannot be done.

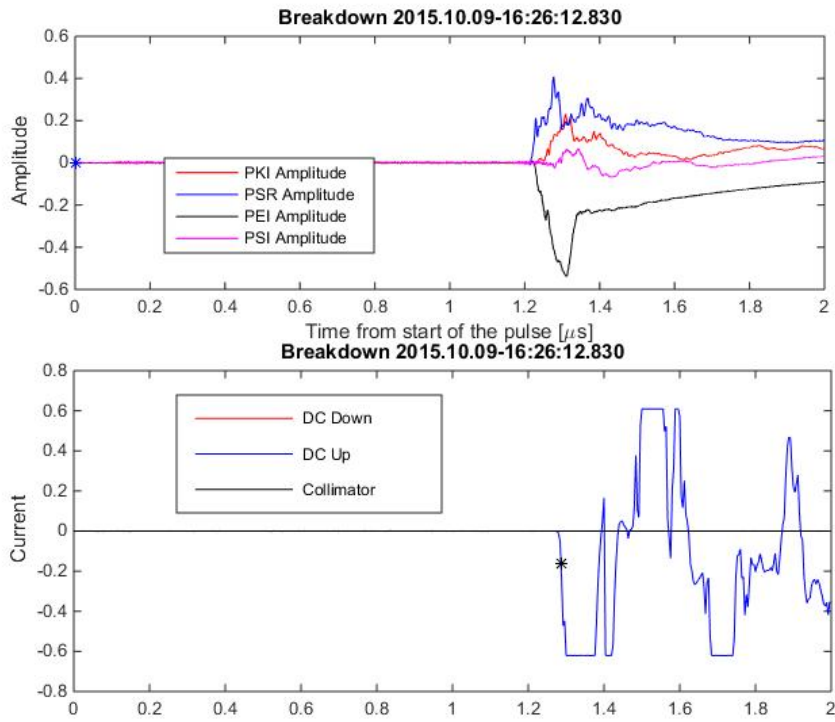


Figure 4.8: Signal when calculating the faraday-cup signal timing. Stars on the RF signals show what positions is chosen from the algorithm.

#### 4.4.4 Phase method

The method described in this section is used to more accurately position breakdowns in the cavity cells. From calculations of the timings of the previous methods, it can be understandable that some inaccurate results will appear. This can be corrected with the use of phase data and the knowledge that there is a  $\frac{2*\pi}{3}$  phase advance per cell.

By first aligning the phases in the same manner as for the method itself and then take the differences between both signals phases, one can find a stable phase. Choosing this phase to be stable enough (have a Standard deviation of the phase by less or equal to 10 degrees) one will find a timing and phase correlation. This then makes it possible to use this information to put irregular positions into correct cells. The phase difference between the incoming and reflected signal should fall into discrete steps separated by the value of the phase advance per cell of the structure namely 120 degrees, Figure 4.9 shows how the results can look but without any cell location information. This is not in this thesis work. See [20] for further information and results.

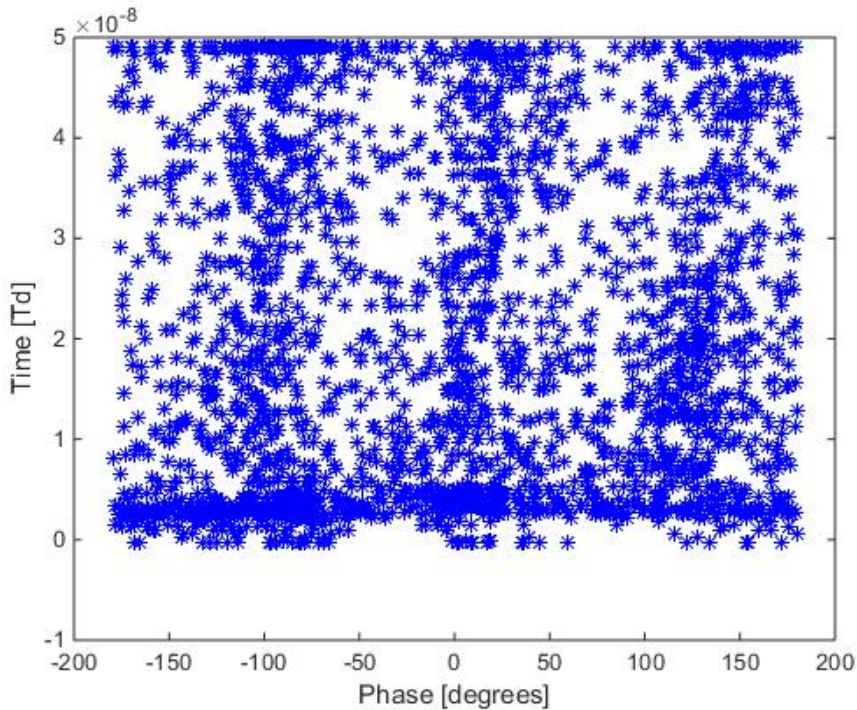


Figure 4.9: Time distribution vs Phase difference for multiple events over the period September - December 2015. It can be seen that most events follow the  $\frac{2*\pi}{3}$  phase advance.

## 4.5 UCXS Images

Image method has been the focus of this thesis.

The collimator has two different positions as previously described, slit and pinhole. Data used for the T24Open cavity started in September 2015 with a slit opening and changed to pinhole in February of 2016. Data used for analyses with slit is for the time period October 2015. Pinhole data used is from February the 24th 2016 - April the 5th 2016. Data used for slits is only for October of 2015 due to the non-optimized gain factor on the camera under September month, making many pictures being unusable. While data from November and December could be used, they were not so many. Only 13 days of events with diminishing numbers due to the conditioning process. Figure 4.10 shows that there can exist more than one spot on the images. This is thought to be due to the breakdowns not originating from a point location and instead from a larger area around the iris. When a breakdown occurs the arc formed from the excess charges is not only going from point to point but rather from an area to another area of the iris. It is also thought that these arcs travels from iris to iris in each cell since the surface field is larger here than in between cell irises. The size of these images could be an indication to where a breakdown occurred in the cavity. This since the magnification to the screen would change depending on position inside the cavity, when knowing the collimators opening size. So the idea would be to measure the height and width when the collimator uses a slit and radius when the collimator uses a pinhole, to estimate the magnification. This can then be compared to cell locations from the RF signal methods to see if any resemblances exist. As seen from figure 4.10 it can be

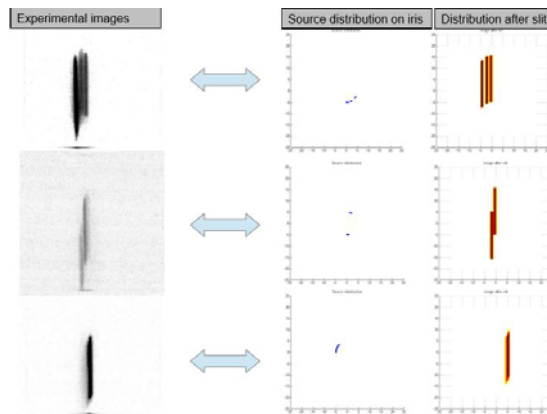


Figure 4.10: Breakdown from different position on iris together with curvature example. Top shows an image with what can be seen as 3 slits. It also shows how this can be interpolated to iris positions. The closer the iris positions are the more the image resemblance a single breakdown. If like on the middle the iris positions are separated in height the slit will look like one longer image slit., from [7]

problematic for an analyse to be done if a breakdown looks as the third event. This since it could be one or more very close breakdowns showing, giving the resemblance to a single spot.

The analysis is divided into four sections. Section 4.5.1 will go through the calibration done before images can be analysed. Section 4.5.1.1 will go through the images and how they are used. Section 4.5.1.2 is how the images are connected with RF analysis. Section 4.5.1.3 is about how the images with multiple features can be used and what hypothesis can be formulated, figure 4.11a and 4.11b shows typical images of a slit and pinhole.



(a) Image taken with slit collimator when multiple features are seen. (b) Image taken with slit collimator when multiple features are seen.

Figure 4.11: Difference between slit and pinhole images

#### 4.5.1 Image Calibration

For both the slit and pinhole an image calibration was needed. Calibration makes use of five markers that are placed on the screen with lithographic method, with the known positions. Figures 4.12 and 4.13 show the process before and after. The picture is resized in height to make the small crosses in each side to have the same length between them. Length between the crosses (as can be seen on figures) in horizontal and vertical direction should be equal. By calculating the number of pixels between the points together with the knowledge that the screen is situated with a 30 degrees angle from the collimator line makes it possible to resize the image to a 50x50 mm image. In this case the image goes from a 1100x600 pixel to an 1001x1001 pixel picture. This means that one pixel will be almost 0.05 mm (0.4995 mm). It is also necessary to rotate the image a little and this is done by using MATLAB's function `imwarp` together with `affine2d` which can be used to resize and rotate images.

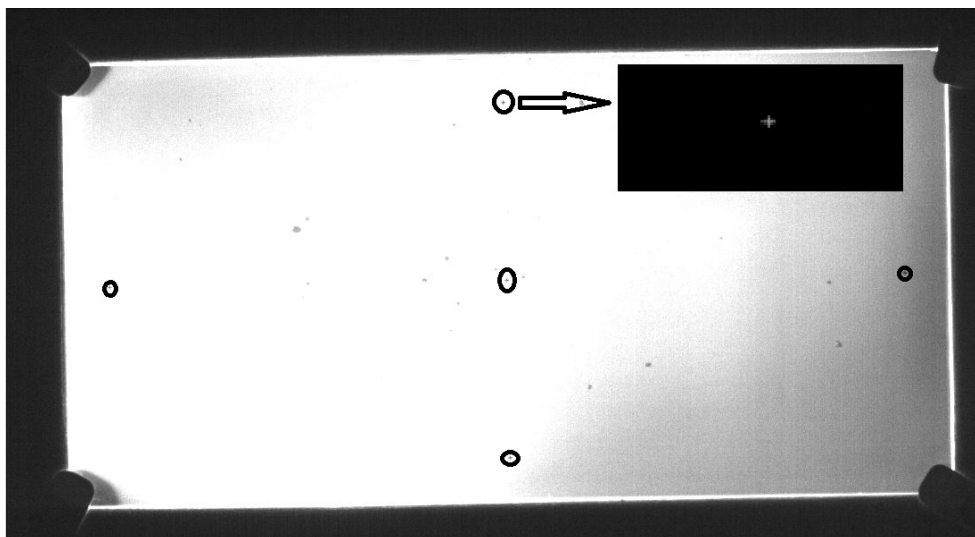


Figure 4.12: Picture of the calibration image before any calibration has been done. Notice small crosses in each directions and in the middle. An inverted image of one of the cross where put in to easier see how the crosses look like.



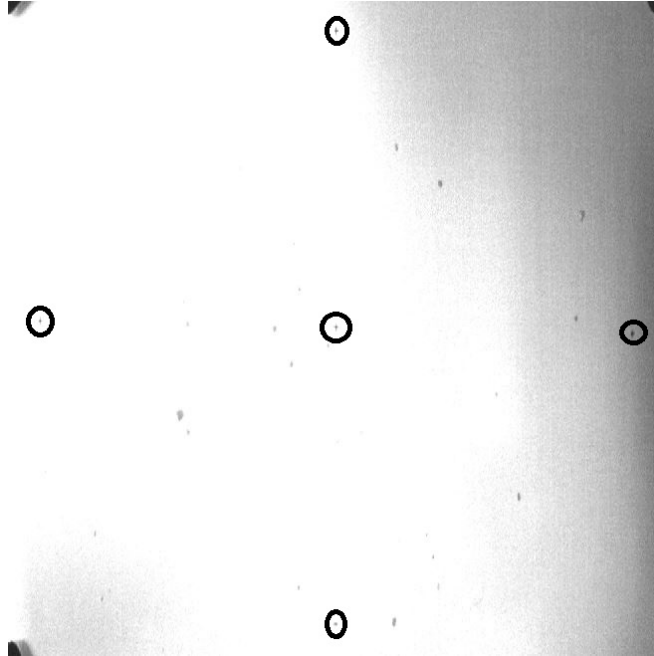


Figure 4.13: Picture of calibration image after calibration.

#### 4.5.1.1 Feature analysis

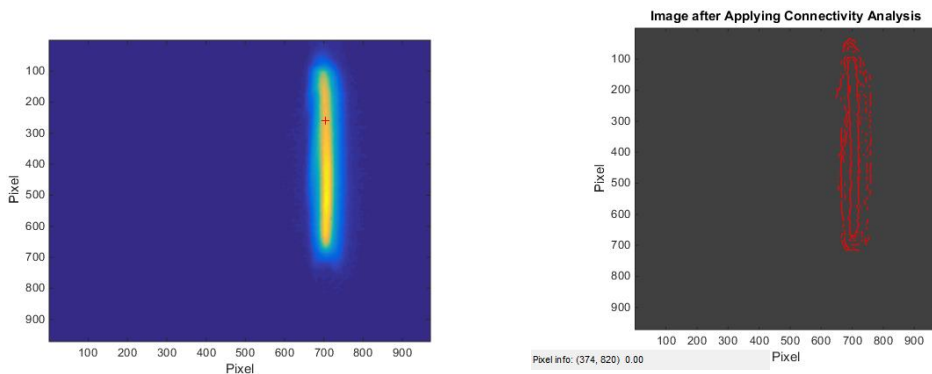
- Slit:

The Slit features can be seen in figure 4.14a. Here the image has a color map used to easier see the target slit. In this figure one can see a small cross. This cross is formed by finding intensity peaks around the target area. When a number of peaks are found, they are used to mark the total number of slits found inside a picture after using a code called FastPeakFind, by Adi Natan. With this function MATLAB finds a lot of peaks. Since all peaks found are not interesting, a cleaning algorithm that removes peaks within a proximity of 15 pixels of each other is used. Only a few peaks is wanted and in most cases this algorithm works. If by any chance crosses appear before 500 pixel value in horizontal direction they will also be discarded. This since a slit position here is unrealistic. This code is developed to be able to differentiate between spots close together and spots overlapping.

Necessary to do next is finding the edges of the slit spots. What is done after finding the number of spots a code called Canny2d by Rafael C. Gonzalez, Richard E. Woods is run. This code find the edges of the given image as can be seen in figure 4.14b. By using a projection over the result from the Canny2d function a plot finding the width is done, as seen in figure 4.15. Here the tricky part can come into play. Figure 4.15 shows a simple two peak plot which makes it obvious where the set edges are and therefore the width. With the algorithm used now multiple different results can be seen and will be summarized underneath.

- 1 Spot with 2 peaks
- 1 Spot with 3 peaks
- 2 Spots with 3 peaks
- 2 Spots with 4 peaks
- 2 Spots with 5 peaks
- 2 Spots with 6 peaks





(a) Counting number of slits seen on the images with the help of a peak finding algorithm called FastPeakFind by Adi Natan. (b) Canny2d edge detection method results. Used to see edges and therefore find width of each slit. Algorithm by Rafael C. Gonzalez, Richard E. Woods

Figure 4.14: Image for slit counting and then how edges look after edge algorithm is used.

- And so on with a maximum of 4 slits found in data. Will be further explained in section 4.5.1.3.

More about multiple features in section 4.5.1.3. What have been seen is that a single slit can have 2 or 3 peak values. This is a problem when trying to find a rule to follow when analysing the images.

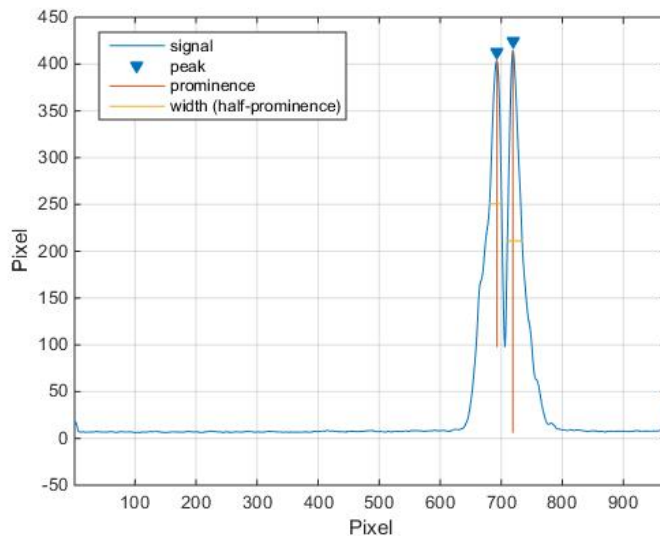
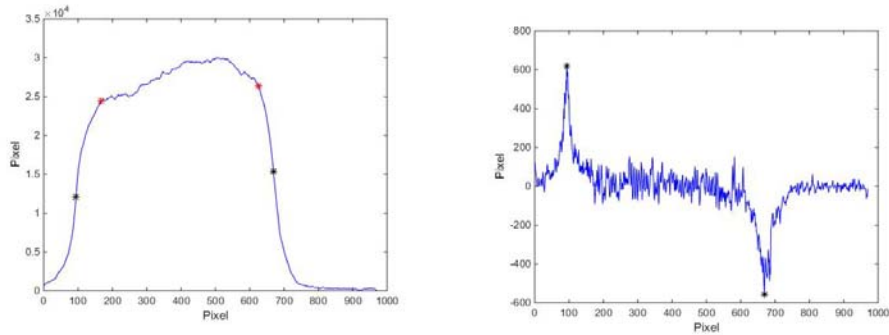


Figure 4.15: Peaks found for seen image. This decides the width of each slit and therefore decides points where a row projection can be done.

After everything is calculated a picture over the image together with the calculated rectangle is shown, like in figure 4.16. This figure is inverted to make the rectangle more visible. The height of the rectangle is calculated from the use of projection of the rows between the points that is the width of the slit. As said before the accuracy is increased by also taking the derivative of the projection and take the maximum slope points as a start and end to the slit height. Projection and derivative plots can be seen in figure 4.17a and 4.17b.



Figure 4.16: Images when slit is used together with calculated size by the MATLAB algorithm. Height of this slit became 28.7 mm (575 Pixels) and the width became 1.3 mm (26 Pixels).



(a) Analysis of the slit images when projection is done on the rows. Black points show where height start and end calculation was done so that points chosen depends on the derivative instead of a randomly set value. Red points show calculated start and end point of the slope.

Figure 4.17: Analysis plots of what points were chosen after algorithm calculation.

- Pinhole:

Unlike the slit algorithm the pinhole will not use an edge detection function. It was decided after some tests that it would be better to make a code where a marker is put on top of a pinhole image spot and from there do a 2-dimensional gaussian fit. It was a hypothesis that the gaussian fit would work even though it did not work for the slit. This since the pinhole intensity spots look more like a gaussian distribution in both directions.

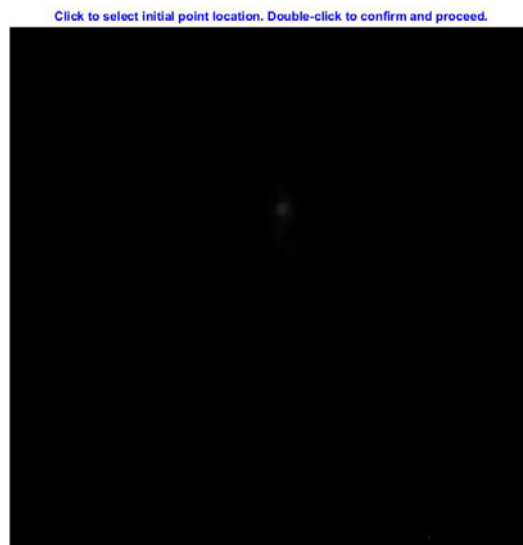


Figure 4.18: Image when given a decision to pin point a position where the algorithm start calculations of size. Pinhole image being very small in comparison to the screen.

Figure 4.18 shows the picture where one will with pointer decide a position where the calculation can start from. Figure 4.19 shows how the algorithm then works for choosing the size of the area. It starts by calculating the 2d gaussian function and then makes an ellipse from the gaussian parameters  $\sigma_x$ ,  $\sigma_y$  and the angle. By starting with a circle of size 15 pixels, it then increases the pixel size each turn and when the calculated area is in the order of less or equal to 2% of previous area it stops. Solution then comes in the form of ellipses as seen in figure 4.20.

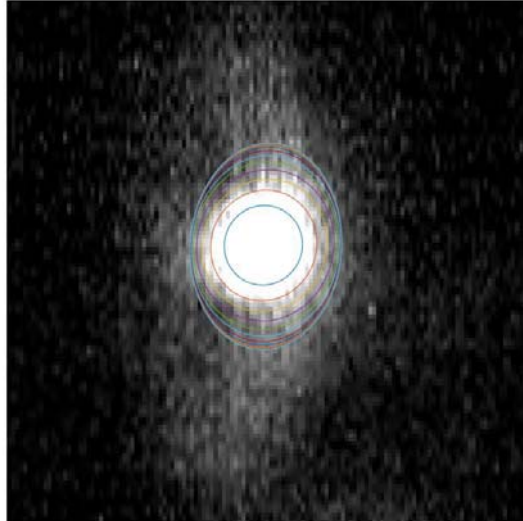


Figure 4.19: Calculation of 2% error uncertainty. Many ellipses is done until the size increase is under 2% and the largest (last) is chosen.



Figure 4.20: Single pinhole feature and the calculated result from MATLAB algorithm.

#### 4.5.1.2 Analysis with RF information

Interesting was to see if the images and their size could be used to calculate together with RF information for each event the position. This would be done by calculating with the edge, correlation or FC method a position for the breakdown, then this would be correlated to the size of the image spot/spots to see what would work best. Since the magnification length was known from figure 4.21 it could be used to calculate the size the image was supposedly going to be when travelling through the collimator and onto the screen.

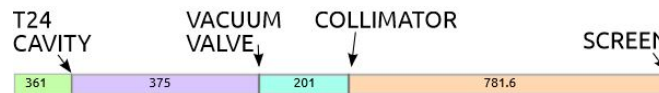


Figure 4.21: Distances used for magnification calculation.

#### 4.5.1.3 Multiple Features

- Slit:

Multiple features are calculated in the same way as the single ones. For slits the algorithm gets longer since the bullet table telling spots and peaks will continue until all different cases are taken into account. Continuing from single features it keeps on like:

- 3 Spots with 4 Peaks
- 3 Spots with 5 Peaks
- 3 Spots with 6 Peaks
- 3 Spots with 7 Peaks
- 3 Spots with 8 Peaks
- 3 Spots with 9 Peaks
- 4 Spots with 5 Peaks
- 4 Spots with 6 Peaks
- 4 Spots with 7 Peaks
- 4 Spots with 8 Peaks
- 4 Spots with 9 Peaks
- 4 Spots with 10 Peaks
- 4 Spots with 11 Peaks
- 4 Spots with 12 Peaks
- Pinhole:

The pinhole calculations are the same as before, with one exception. This is to use an algorithm that makes the area of a previously calculated spot totally black for next pinhole spot in same event. This gives problem for spots that are in neighbourhood to each other. Knowledge of how many spots exist has already been given since one still needs to point out how many ellipses that needs to be calculated. There is usually a good agreement when the correct amount of spots are chosen.

Calculation of the ellipse is only inaccurate when spots are too close to each other. This since calculation of the ellipse region enters a new spot during calculation. When the calculation enters the region of another spot

the algorithm will keep on looping. This is because the size will start to grow when a new high intensity region is present. By making previously calculated spots black after calculation this can be avoided for some spots. It still will not avoid areas calculated for the first time where two spots are close. Therefore it possible to discard calculations that enter black areas but not calculations that has entered spot areas before any calculation has been done in that region, see result section 5.2.3.

# Chapter 5

## Results

This chapter will show the analysed results together with discussion on what exactly is seen, and how this can matter for future breakdown analysis.

First longitudinal positioning from the three different methods and their distribution will be discussed, followed up by image analysis results.

### 5.1 Results Longitudinal Methods

#### 5.1.1 Edge Method

Using the information of RF signal timings a histogram plot was made in order to see where most breakdowns seem to occur and if this has anything to do with the conditioning process explained in section 2.1.4. From the

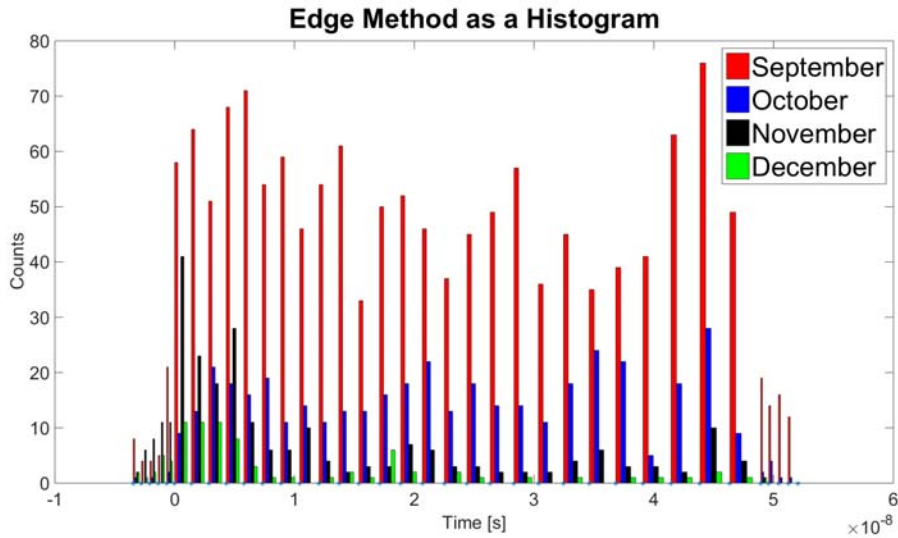


Figure 5.1: Time distribution for data calculated by the Edge Method

histogram it can be seen that the distribution of breakdowns is symmetrical. Each bin is equal to the time it takes for the signal to travel through the different cells, in total 24 cells plus two extra cells for input and output. Bins outside of the filling time 0 - 49.5 ns is used for breakdowns outside of the cavity where the group velocity is much higher, making the width of the bins very small. The CLIC crab cavity distribution is not as symmetric. This is mainly due to that the T24OPEN cavity is a constant gradient structure while the Crab cavity is a constant

impedance structure. This mean that the electric field in the T24OPEN is constant throughout the cavity and since breakdowns have a higher chance to occur where there is a higher field the structure T24OPEN will have a smoother distribution. See figure 5.3 for the crab cavity correlation distribution.

### 5.1.2 Correlation Method

Figure 5.2 shows the same distribution as for the edge method but now for the correlation method. What can be seen is something that looks like a migration towards earlier cells. It means that breakdowns occurs with a more frequent rate in the early stage of the cavity. Figure 5.3 shows the same distribution of with correlation method for the Crab cavity. For the Crab cavity however we know that there should be a higher BDR in the early stages of the cavity.

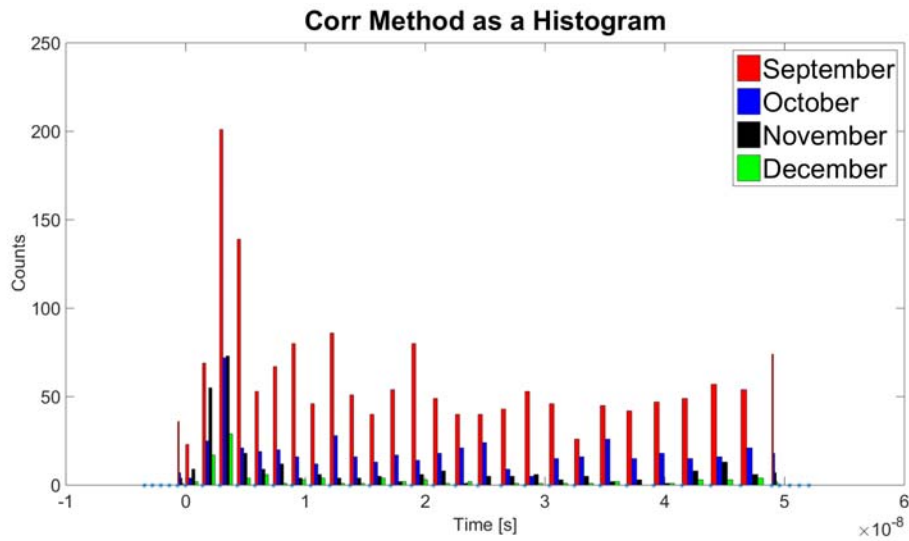


Figure 5.2: Time distribution for data calculated by the Correlation Method.

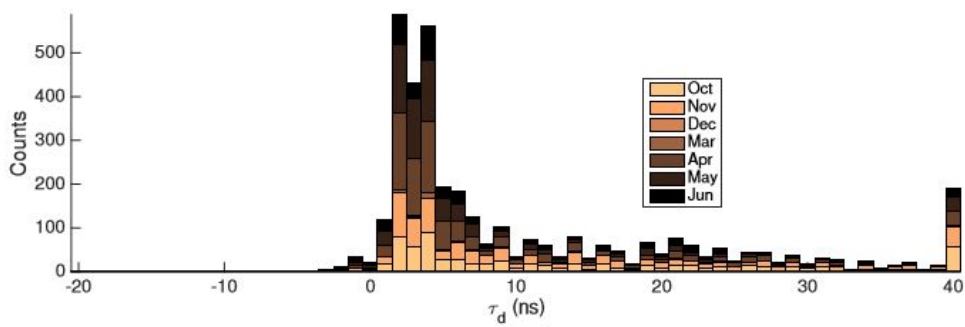


Figure 5.3: Distribution of breakdowns throughout the CLIC crab cavity using the correlation method. Note that the time on X-axis is double from what results used in this thesis work. From [20]



### 5.1.3 Faraday cup Method

In figure 5.4 we see that the same distribution as for the edge and correlation method. There seems to exist an offset of around 10 ns, which is most likely due to the alignment problem which exists for the faraday-cup method. There was a hope to use the new signal from the BLM to align the signal but this has not yet been successful.

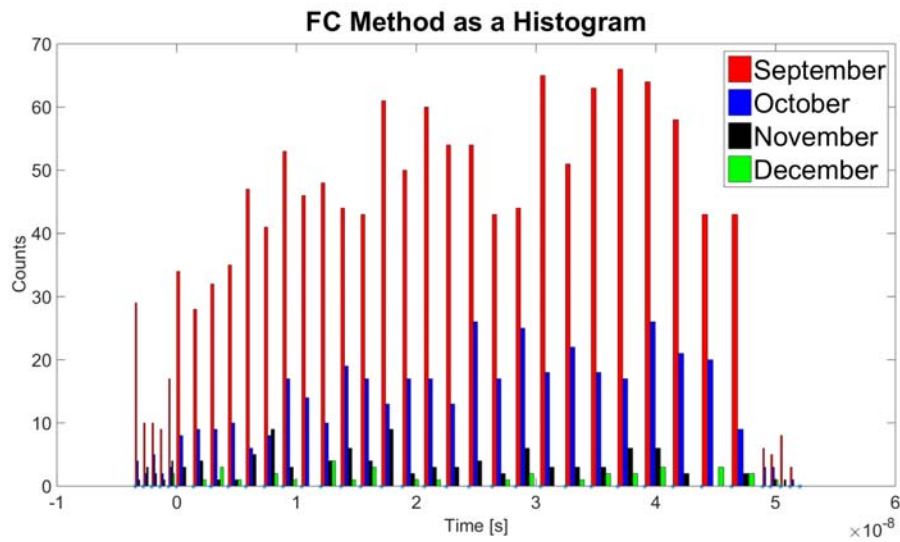


Figure 5.4: Time distribution for data calculated by the FC-Method

### 5.1.4 Difference

Here we can see the distributions of the difference between the methods. In Appendix A there will also be scatter plots between the different methods, for further illustrations of the difference.

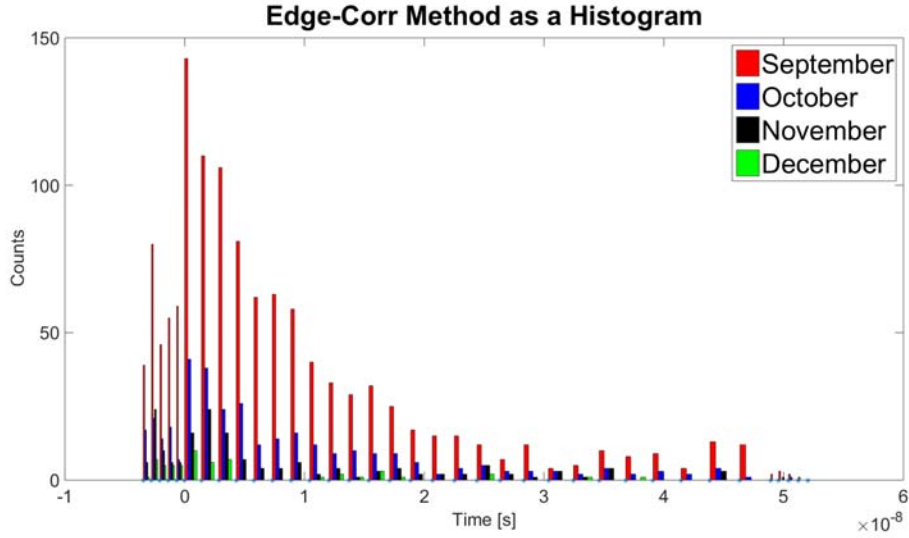


Figure 5.5: Time distribution for the difference between Edge and Correlation method

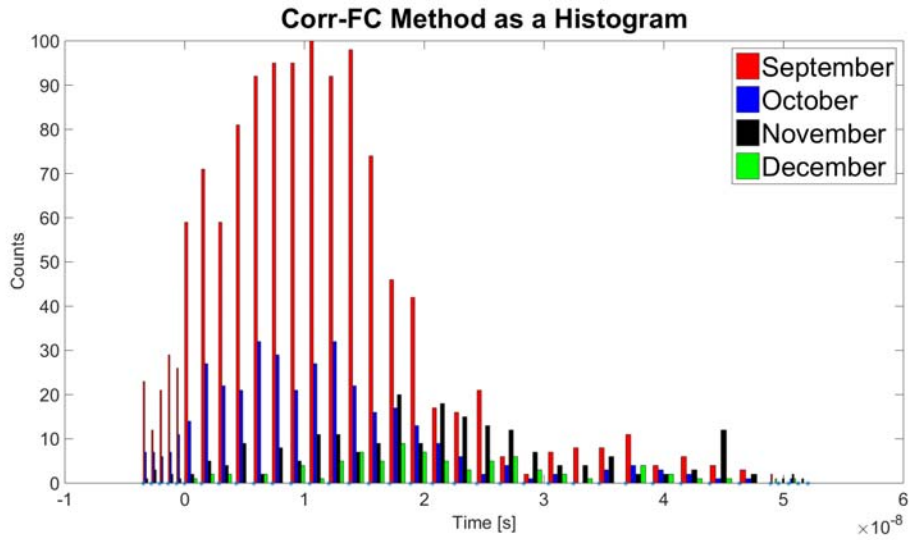


Figure 5.6: Time distribution for the difference between Correlation and Faraday-cup method

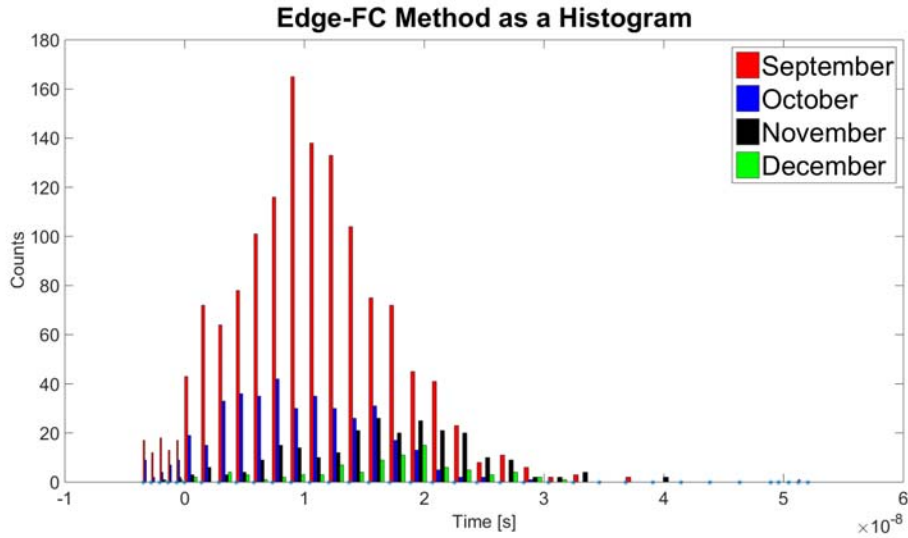


Figure 5.7: Time distribution for the difference between Edge and Faraday-cup method

The three difference distributions show that a resemblance between the correlation and edge method exists, where faraday cup method has an offset. Even though there is a difference between the distribution of edge method and correlation method the difference has a gaussian like curve around 0. This could be misdirected since there has also been an increase in events happening before the time 0. The breakdown migration, which is the big theory when discussing correlation method seems to exist in this result as well. Another theory which could explain the asymmetry between the edge and correlation method would be breakdown formation happening further upstream. This means that RF power still exists after a breakdown event have occurred (which have been seen) would produce another breakdown. Since both edge and correlation method only can calculate one location, this means that if two breakdown occur under the same event they can give a result from different breakdowns. Correlation will only take the best correlated signal which might be the second one, while edge method calculates the first one. It can also be mentioned that faraday cup method without knowing the alignment inaccuracy, show a close resemblance to the edge method distribution. It means that the faraday cup method would also only calculate the first breakdown in an event. This is further strengthened by watching the difference between the different distributions including faraday cup method. There seems to exist a small migration towards earlier cell location when comparing faraday cup and correlation method, which once again tells that correlation method show signs of migration.

More data showing these distributions is important for monitoring condition processes. This to prevent developments of "hot cells", cells where many breakdowns will occur. Hot cells could lead to damage of the mechanical structure in such a region.

A few examples were picked to see how close of a resemblance a few events have when going through the different method algorithms. They are shown in table 5.1, but no clear resemblance can be seen. Some events have a close resemblance while other differs a lot. This can be because different methods calculates different breakdowns in the same event.

Table 5.1: Method Comparison

Number of spots\Method	Edge	Correlation	FC
1 Spot	18.765 [ns]	24.015[ns]	4.150 [ns]
1 Spot	3.140 [ns]	3.078[ns]	-18.500 [ns]
2 Spot	20.328 [ns]	4.015 [ns]	5.025 [ns]
2 Spot	50.015 [ns]	37.140 [ns]	33.775 [ns]
3 Spot	24.073 [ns]	8.078[ns]	18.150 [ns]
3 Spot	28.765 [ns]	30.890[ns]	25.650 [ns]

## 5.2 Results from UCXS Images

### 5.2.1 Features

The total number of breakdown events together with total number of usable events for both collimator openings is summed up in tables 5.2,5.3. Slit and spot mean how many image spots that can be seen on the image. Working images is how many images that are clear enough to show an image spot. Discarded events for the slits means that the calculated height gets too close to the edge of the picture, in this case 5-pixels or 0.25 mm. Perfect images are images where nothing have had to be discarded. As can be seen the percent of used images is low, which came as a surprise when results were presented.

Table 5.2: Table over Slit images October 2015

Number of Images	590
Number of Working Images	242
Number of Non-Working Images	348
Number of Slits	387
Number Discarded Slits	265
Number of Perfect Images	84
Number of images with 1 spot	105
Number of images with 2 spot	94
Number of images with 3 spot	39
Number of images with 4 spot	4
Number of images with 5 spot	0
Number of One-Discarded-Slit	82
Number of Two-Discarded-Slit	51
Number of Three-Discarded-Slit	19
Number of Four-Discarded-Slit	6
Number of Five-Discarded-Slit	0
Number of Higher-Discarded-Slit	0

Table 5.3: Table over Pinhole images February 2016 - April 2016

Number of Images	448
Number of Black Images	223
Number of Good Images	204
Number of Bad Images	21
Pinhole Spots	340
Pinhole Spots on good Images	292
Pinhole Spots on bad Images	48
Pinhole Images with 1-spot	139
Pinhole Images with 2-spots	47
Pinhole Images with 3-spots	14
Pinhole Images with 4-spots	3
Pinhole Images with 5-spots	1
Pinhole Images with Higher-spots	0

### 5.2.2 RF-Signals

When trying to correlate the image sizes with RF signal timings, a table was done to see how different methods from the RF signals correlate to each other. This table can be seen in 5.1. Using the magnification factor calculated from the distances (which are close to 1) it was easy to understand that this type of analysis could not be done. Almost every image is larger than the maximum magnification size. An example is for a certain pinhole image the size of the ellipse can go up to 25-30 pixels which would correspond to 1.5 mm in major or minor axis. 1.5 mm would correspond, since the collimator hole is 0.5 mm in diameter a magnification factor of three times as much and since the magnification maximum is close to one the hypothesis on these images had to be neglected. Figures 5.8, 5.9 and 5.10 shows with two different timings before 25 ns and after 25 ns (since filling time of the whole cavity is 49.5 ns) how high the image spot is when the timing is long or short. The timings mean where inside the cavity structure the breakdown occurs. Before 25 ns means before a little more than half (since the signal velocity is faster in the start), while after 25 ns means the last part of the cavity. As can be seen there is no chance to know where

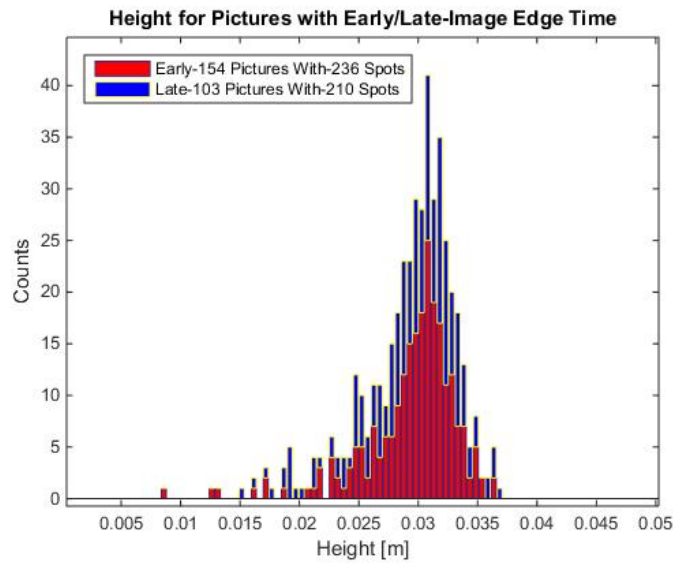


Figure 5.8: Histogram over the height of image spots for two different timings, after 25 ns and before 25 ns.

in the cavity a breakdown has occurred, by measuring the height of the slit spot. This is not what was hypothesised in the beginning of this thesis work. To be able to localize a breakdown from images someone either has to develop an improved algorithm to calculate a more exact size of the image spot, or a new hypothesis has to be formulated.

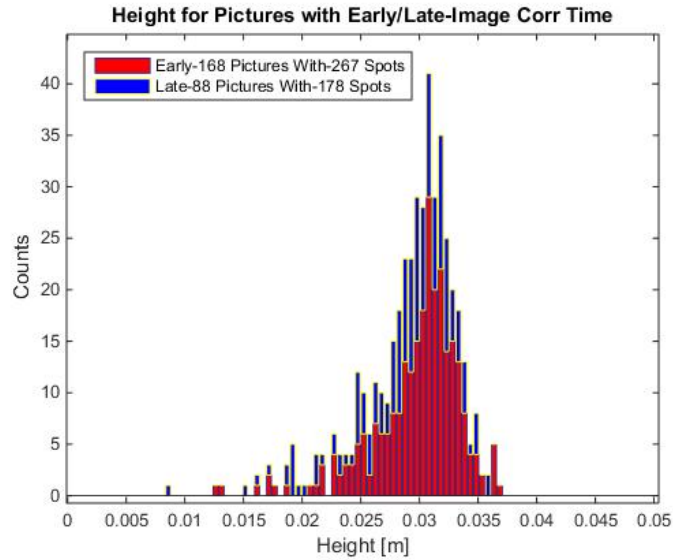


Figure 5.9: Histogram over the height of image spots for two different timings, after 25 ns and before 25 ns.

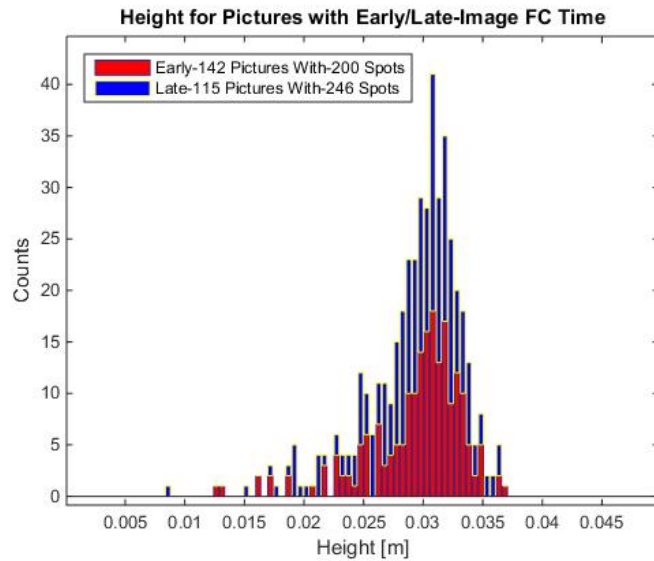


Figure 5.10: Histogram over the height of image spots for two different timings, after 25 ns and before 25 ns.

### 5.2.3 Multiple Features

Figure 5.11 shows an example of a 3 slit calculated problem with 3 different rectangles. It can be seen from the figure that the algorithm that treats the slits work. From 5.2 we can see that many image spots had to be discarded even though a good rectangular shape were calculated. This was since we cannot use image spots too close to the edge because of unreliability. These spots could have been larger than calculated since they have to be cut on the edge. This gave the idea that when possibility exist, one could move the screen slightly. This would make these

events appear well on the screen and since no events have ever been close to the other edge it would work well.



Figure 5.11: Images when slit is used together with calculated size by the MATLAB algorithm.

Figure 5.13 shows the result after using this algorithm on the picture from figure 5.12. It can be seen that there are only three ellipses with enough size. There actually exists a fourth, if one zoom in enough but this ellipse will be discarded due to overlap from previous calculation.

[Click to select initial point location. Double-click to confirm and proceed.](#)

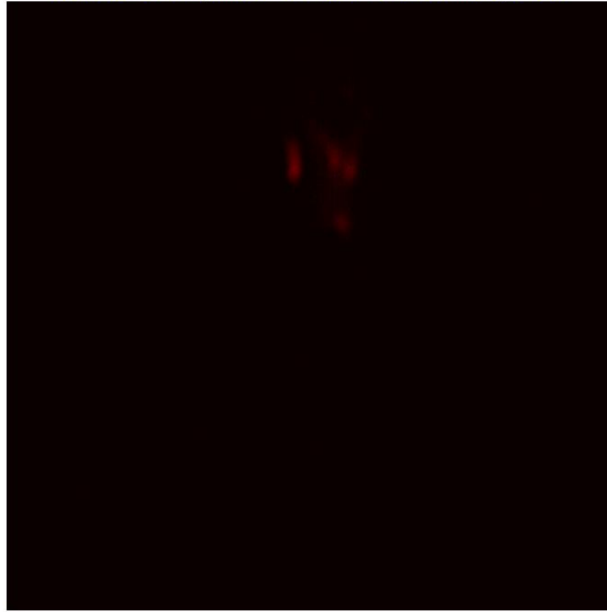


Figure 5.12: Image when given a decision to pin point a position where the algorithm start calculations of size.





Figure 5.13: Multiple features after calculation. As can be seen only three points can be chosen with good results, while the last will be discarded due to overlap

Figure 5.14 shows how the two 2D-gaussian sigmas, meaning the different minor and major axis of the ellipses changes. It can be seen that  $\sigma_y$ , meaning the size in y almost always is larger. This is something that is unexplained and should not happen. Why this can happen might be due to algorithm/calibration error that makes the screen give an inaccurate size appearance. However similar results have been seen in Uppsala before which makes it even more interesting.

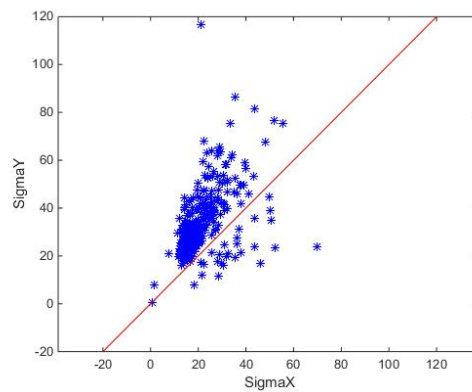
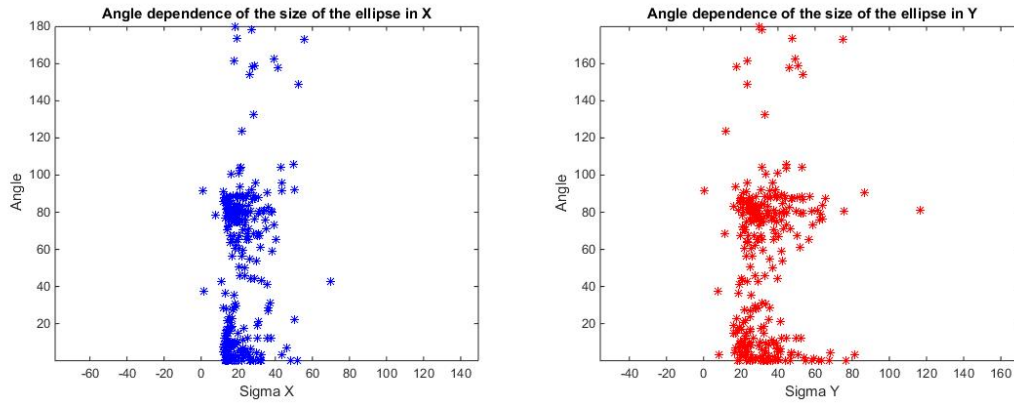


Figure 5.14: Sigma for both direction for all pinhole events.

Figures 5.15a and 5.15b show plots over the angle dependence versus the 2D gaussian distribution parameters  $\sigma_x$  and  $\sigma_y$ . The angle here is the angle of the ellipse and describes how it need to be angled in the images to fit the image spots. Both sigma values have equal values when compared to the angle, so both have equal or no correlation at all with the angle. This gives a statement that there exist breakdowns all over the cell irises, due to the wide range of angles the different events have. No angles exist around 45 and above 90 degrees. Distribution for the angle and sigma's can be found in appendix A.



(a) Angle vs sigma X for all pinhole events.

(b) Angle vs sigma Y for all pinhole events.

Figure 5.15: Angle vs both sigma directions

The next figure 5.16 shows the cumulative distribution of all 340 pinhole image spots mean value in both directions. Two circles are drawn in the plot. They indicate an iris with two different sizes. The small size is 7 mm which would be around the maximum size of an iris when magnified, while the large is 10 mm and would simulate an iris focused on having pixel deviations accounted for.

The figure indicates where the breakdowns can occur in the iris. Since this data seems reliable together with the magnification factor one could use this data when opening cavities too see if these positions are where breakdowns occur. Still many events have to be discarded due to either being very dark images where the breakdown spot cannot be seen, or due to errors in the RF signal. This data could also be used by normalizing the data to a set iris radius and then calculate the different radius of the events. This is one way to calculate the center of the cavity which could be used for improving beam position.

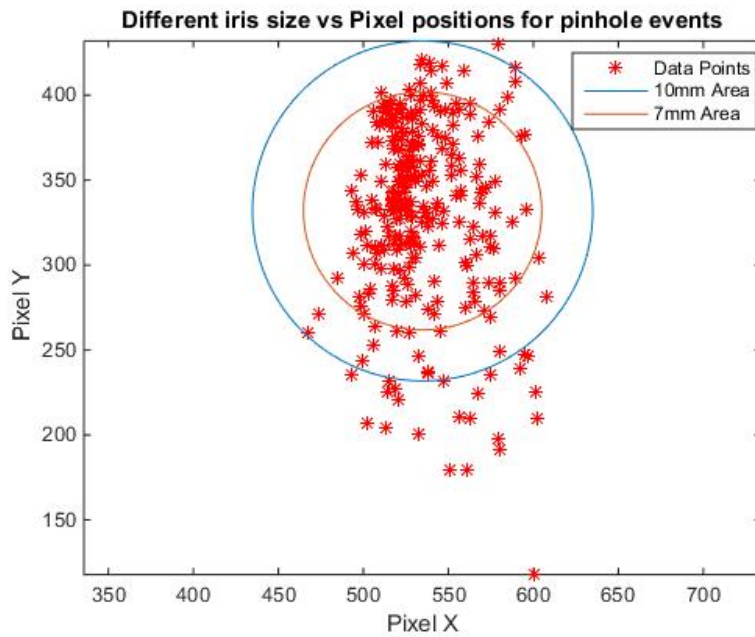
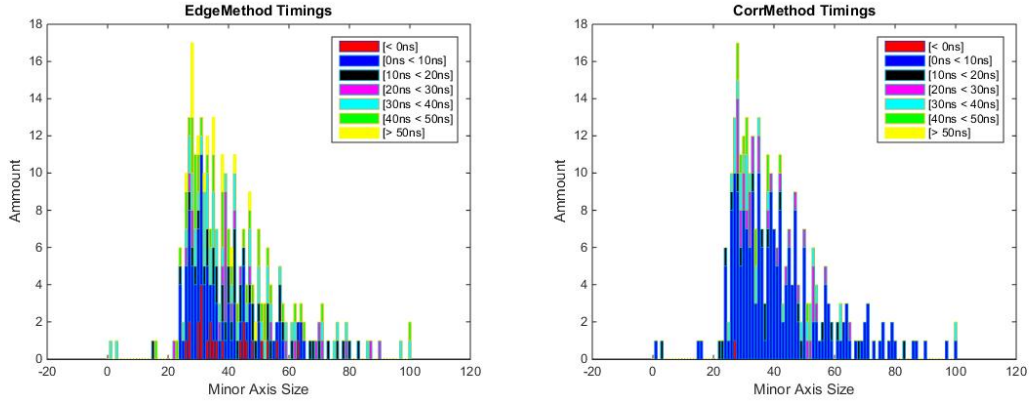


Figure 5.16: Mean value positions for all pinhole events, together with two different iris sizes. 7 mm would be for an iris of the correct maximum size while 10 mm is to include position deviations.



(a) Edge method distribution over minor axis size depending on calculated RF timing, for all pinhole events. (b) Correlation method distribution over minor axis size depending on calculated RF timing, for all pinhole events.

Figure 5.17: Distribution for correlation and edge method for pinhole events.

As for slit events, a distribution plot was done for all the pinhole events. This time more timings were used to see if there was any chance of finding some correlation, in order to calculate the breakdown position longitudinally. Important to note is that the size measured is the minor axis. This since it will always be the minor axis that is of interest when trying to calculate backwards to the breakdown location. Minor axis will always be the axis referring to the iris circle disk height, which should have a maximum value it cannot go above. This since the discharge can go around the iris disk but not transversally for a longer distance. Figure 5.17a and 5.17b shows these distributions. As can be seen nothing can once again be said about the breakdown cell positioning inside the cavity. The timings calculated from edge and correlation method show no resemblance to where in the cavity the breakdown occurs.

## Chapter 6

# Summary and Outlook

In this chapter we give some concluding remarks concerning the thesis. We indicate improvements that can be done and suggest future studies of the breakdown problem. Ideas on how to improve and use the work will be given together with future realistic ways to keep on the breakdown studies and analyses.

### 6.1 Conclusion Breakdown Positioning

#### 6.1.1 RF-Positioning

RF-positioning shows good results when compared to previous analyses. Edge method and faraday cup method both show symmetric results, even though an offset of about 10 ns exists for the faraday cup method. Correlation method seems to have many breakdowns going towards earlier cells inside the cavity. From the distribution this migration looks like it can be up to 10 ns translating to about 3 cells. This asymmetry can have different causes. One being the loss of energy that can be seen for events where the transmitted signal together with reflected are lower than the input signal. Which would make migration occur since the energy needed for breakdown to start would happen later than if no energy would be lost. It can also depend on the turn-on time for the breakdowns which is about 10 ns [20]. The later seems to be a more reliable answer since this happens all the time and can make the correlation calculation differ more, this due to the nature of its mathematics. Data seems to be in order and looks like previously done results, see [20].

#### 6.1.2 Image analysis

From image analysis it can be said that an accurate positioning localisation is hard to achieve. This is mainly because it is hard with a high enough accuracy to calculate the size of the slit or the pinhole spots. The spots on the screen does not seem to follow an imaging magnification and further analysis needs to be done to understand how one could use the size for longitudinal localisation, if it even can be done. This is why this thesis have developed parameters, such as counting of spots and for pinhole the total number of accumulated events, with their mean position location plotted. This has been understood to be very important for further analysis and could be used to calculate the cavity center. It has also been noted that almost all image spots have a larger size in y-direction. This could be because of many different effects, such as charges being gathered on the collimator edges or that the screen have effects that is shown in only y-direction. The theory that more than one discharge can occur under a breakdown event has been further encouraged by the work of this thesis. Discussion to why a single slit can have more than 2 peaks has been discussed before and can be because of a process where breakdowns on the cell iris come from a curvature like position instead of single points. Images where spots are close together but can be clearly differentiated from each other have been seen a lot and adds more to this theory.

When opening cavities and looking inside after the process of conditioning. It has been noticed that there exists more breakdowns than breakdown events counted, it has been theorised that more discharges might have occurred for many of the breakdown events. Results from this thesis agrees with this theory.

## 6.2 Future Work

There is a lot of future work that is needed to further improve the understanding of breakdown physics. This section will go through what the author has seen can be used to further increase the possibility for more accurate analysis of breakdown physics and positioning inside structures under test.

### 6.2.1 Improvements

An improved accuracy in the evaluations of the timings can be achieved by implementing the phase method correction. This could mean that positions such as the second row in table 5.1 could be closer. There still exist values which would not be corrected due to the large difference, so something more has to be part in the improvement.

The faraday cup method seems as a plausible method for further analysis. Finding a way to properly align the signal would most certainly give better result. This can hopefully be accomplished with the new BLM monitor since it measures the signal at all times. To align a signal, it needs to be properly measured even when no breakdown is present and this cannot be done with the other RF signals.

For future work with the UCXS an improvement of the screen position would be necessary, especially with further use of the slit collimator opening. Many image spots had to be discarded due to them being too close to the edge of the screen. This is something that can be done but is harder than what one could expect. It is important to be careful to not break anything and keep the alignment of the other parts of the setup. There are plans to put in a second camera that can be used for images under non breakdown events. This to further see if dark current can be seen when a higher gain is used on a second CCD camera. As previously explained using a high gain will under breakdown events make images useless due to the excess light. By having more information of the dark current and see those images, it is theorised that new information could be seen, where charges gather to form plasma for example. One could also see if there exist smaller discharges that are not measured due to not being strong enough for breaking the threshold limit. All of this could be used to further understand the y-direction smearing that has been seen in the images.

The newly installed BML will be used mainly for radiation control but can be used for breakdown studies as well. What is suggested is to use the low cost optical fibre detector around the structure. Since these fibres are of such low cost in comparison to other equipment they would also be useful for a larger, maybe even a whole accelerator complex. They are also insensitive to neutral radiation which is particles with no charge. Another idea for this is to couple fibres to each cell of the structure. With this it would be possible to see light flashes when breakdowns occur at a specific iris and from there know at which cell this happened by having each signal go to separate feeds.

## 6.3 Contribution

The author's contribution to the breakdown analysis has mostly been through work on UCXS together with small finding on the data acquiring system of X-Box2. Images received from the UCXS is analysed by Uppsala and is therefore something that has been in focus. This work needed to be done sometime and as a master student it was a perfect opportunity to both learn and experience scientific work like this. The dipole magnet situated at UCXS has recently been tested and started to give results. This thesis work has been important for the preparation of using this magnet. By knowing more about the images and having formed a catalogue for different features, this information can be very helpful for the reconstruction of the electron energy that the dipole magnet work will try to achieve.

## Chapter 7

# Acknowledgments

### 7.1 Acknowledgments

I would like to thank the people at the Department of Physics and Astronomy for accepting and letting me help and work together with the experienced people in the CERN group. Extra thanks goes to Marek Jacewicz, my supervisor from Uppsala University, who has given me a great working experience in both learning and discussing problems and new hypotheses. I would also like to thank the X-Box group at CERN that has provided me with most of the information that is used in my work. They also gave me the opportunity to join my supervisor to Mini-MeVarc, a workshop for people working in high gradient research and X-band RF technology.

# Appendices



---

## .1 Appendix A

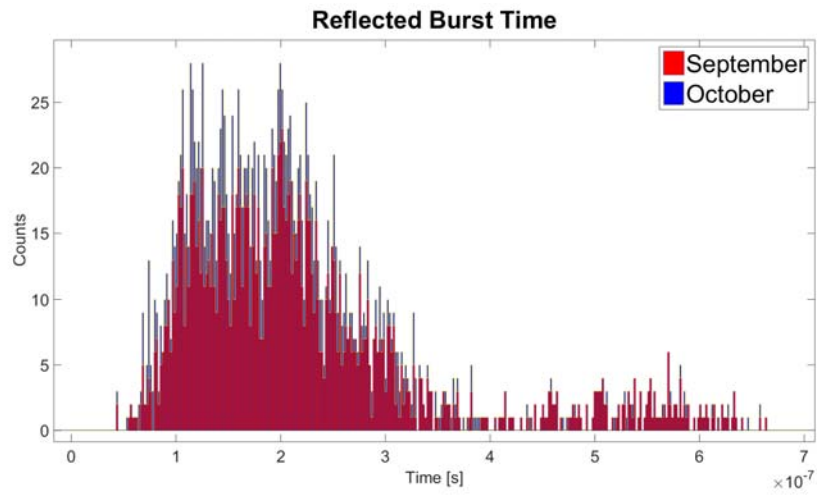


Figure 1: Distribution for the time September-October 2016 for the structure reflected amplitude signal.

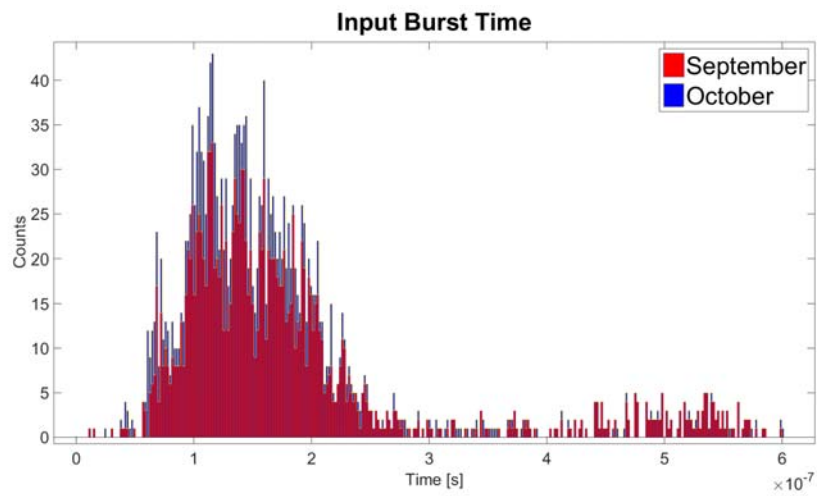


Figure 2: Distribution for the time September-October 2016 for the structure input amplitude signal.

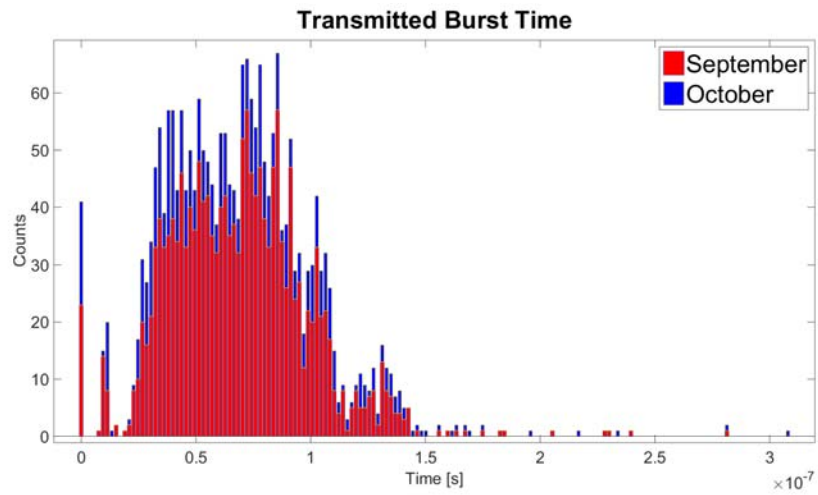


Figure 3: Distribution for the time September-October 2016 for the structure transmitted amplitude signal.

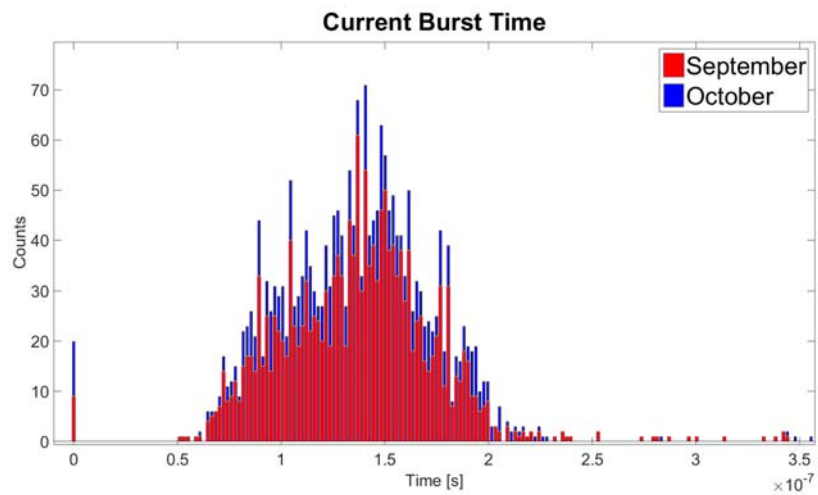


Figure 4: Distribution for the time September-October 2016 for the faraday-cup downstream signal.

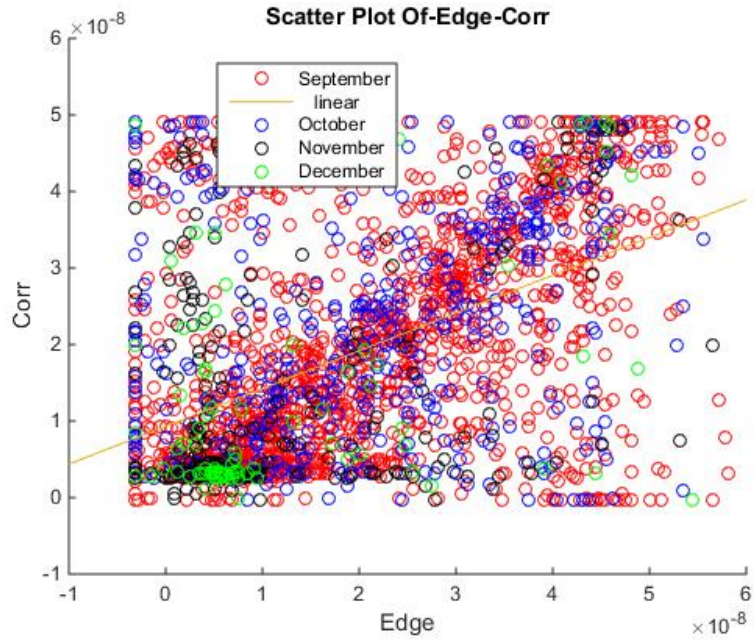


Figure 5: Scatter plot between the Edge and Correlation methods.

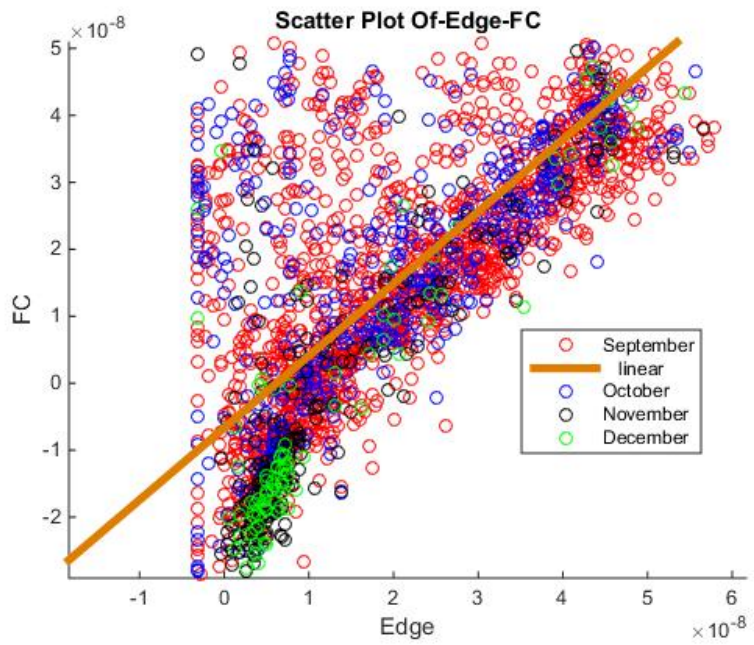


Figure 6: Scatter plot between the Edge and FC methods.

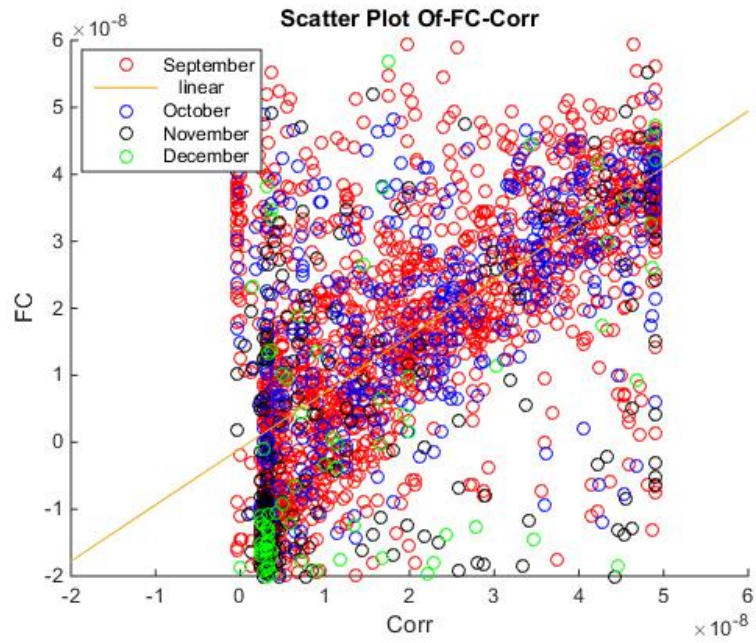


Figure 7: Scatter plot between the Correlation and FC methods.

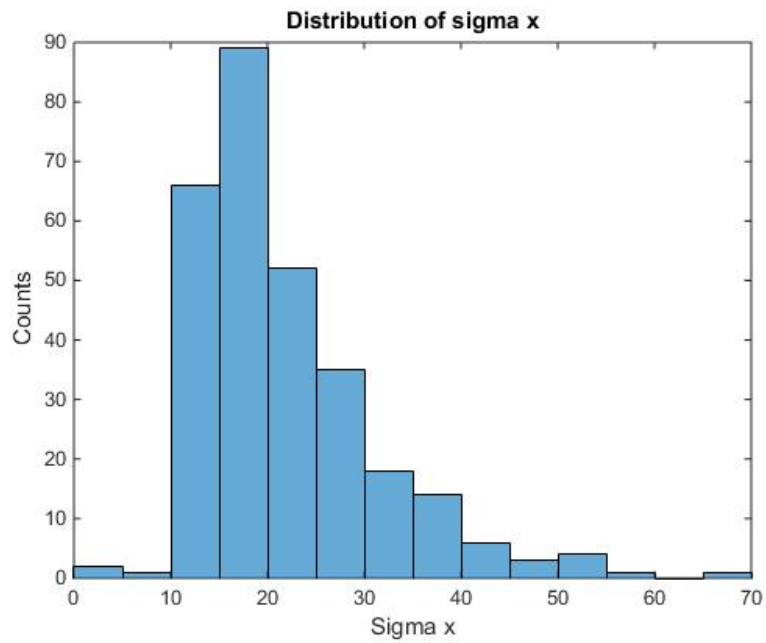


Figure 8: Distribution of sigma x of the pinhole ellipses as a histogram.

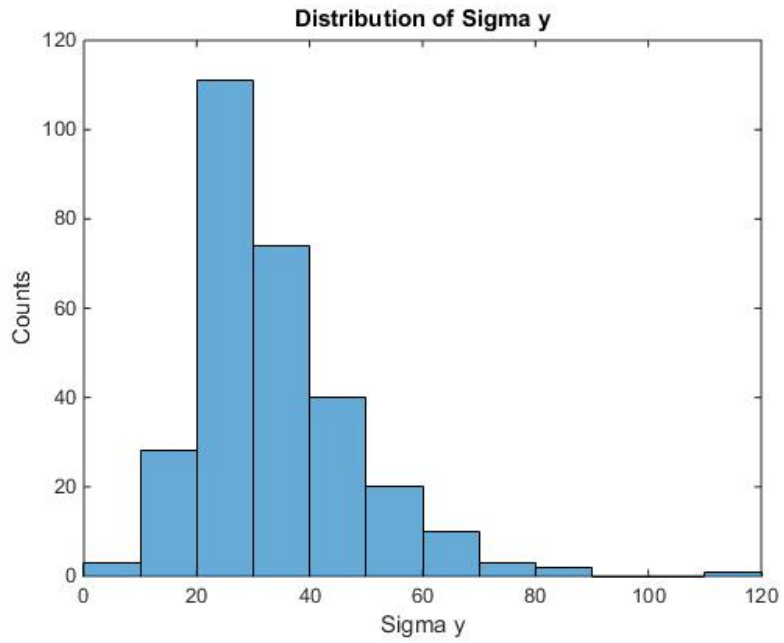


Figure 9: Distribution of sigma y of the pinhole ellipses as a histogram.

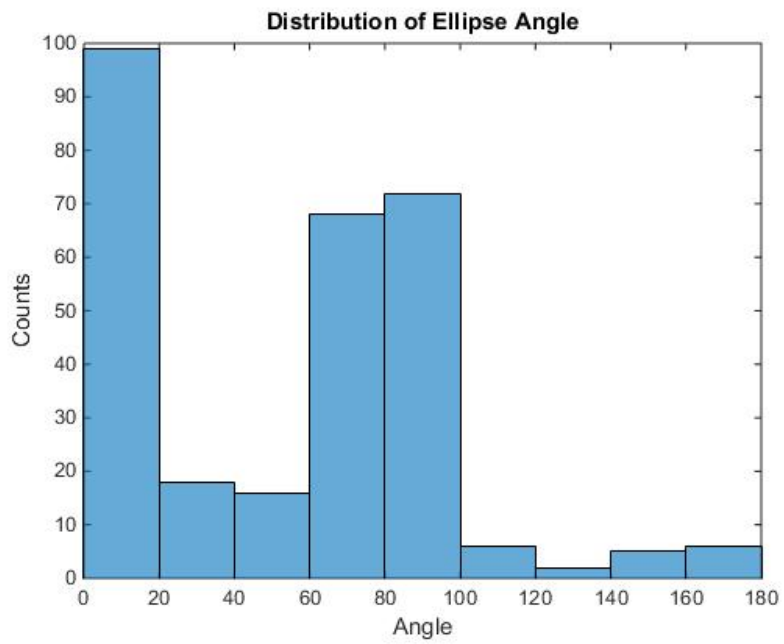


Figure 10: Distribution of the angle of the pinhole ellipses as a histogram.

---

## .2 Appendix B

Main script used in MATLAB where all the different functions are run from.

```
%Main Script
% This Matlab code will use 4 different conversion programs to convert 2
% different fileformats into 1 useable MATLAB format. All folders and files
% will be created automatically. What needs to exist before is a map with
% TXT files which is then called and will need to be located in the
% dictionary of MATLAB. It's of most importance to be sure to have the
% correct dictionary.

%First one is ConvertTDMS into MATLAB and is a downloadable file that
%converts TDMS files into an easy to use MATLAB structure.
Save = true;
Filename1 = 'EventData_20160301.tdms';
[ConvertedData, ConvertVer, ChanNames, GroupNames, ci]=convertTDMS(Save, Filename1);

%Second one is self-made and converts the already converted TDMS file into
%a MATLAB format that can be merged with the MATLAB format made from TXT
%files
%Load the Day you want to convert to multiple event based files
%Example for EvenData from 20151009, str = 'EventData_20151009.mat' where
%'EventData_20151009.mat' is converted using convertTDMS
str = 'EventData_20160301.mat';
LoadAndSaveDataTDMS(str);

%Third one is a conversion from TXT files into MATLAB files. Here all TXT
%files will lie in the same map and be converted without having to change
%file name.
%To load and save from txt format use a string 'str' for the folder all the maps with text w
%Example str = 'Examensarbete/slit1'; %Load from map with BreakdownEvents.
%Where DataSpectrometer have all maps named as date and time like '20151012-063557.97'
str = 'DataSpectrometer';
LoadAndSaveDataTXT(str);

%Fourth and last converter will convert all given convertedTXT files into a
%combined TDMS and TXT format. Why it will be done for all TXT files is
%because TDMS already have files not connected to a breakdown since it has
%data from every minute as well.
%Load in a Breakdown from the DataSetsTXT and connect it to the same
%Breakdown in TDMS
%Write Directory for where TXT formats is. And Connect will be for all TXT
%files if TDMS and TXT.
str = 'DataSetsTXT';
ConnectAllTXT(str);

%If DataSetsTDMS is sent in one will connect the data of breakdowns from
%only a TDMS file not including any pictures
str = 'DataSetsTDMS';
ConnectAllTXT(str);

%
%SingleEventPlot will plot all 16 data sets in one graph including the
```

---

```

%transformed picture with and without the use of a median filter. Pictures
%needed.
SingleEventPlot(strpeak1);

%
%ComparePlot will compare 2 breakdown events in the form of amplitude and
%phase plots, disregarding the log data and faraday up data. Will also
%compare the pictures without any filter. Pictures needed.
ComparePlot(str4, str9);

%
%Use EventPlotBackground with method to calculate longitudinal position.
%Method 1 = PEI falling vs PSR rising
%Method 2 = PSI falling vs PSR falling
%Method 3 is a method to check for the burst of dark current and relate this
%to the falling PEI value.

%EventPlotNoBackground can be used alone to plot a breakdown subtracting
%the background given from the TDMS data. method will decide which method
%that will be used and plot the position this method find. 'Yes' or 'No' is
%to decide if one wants the plot or not. 'No' is used in other codes to
%only use the background data.

EventPlotNoBackground(str4, 1, 'Yes');

%Function to check times for all 3 RF-methods
MethodTimeCheck(str8)

%RegionOfInterestSingleEvent is a algorithm calculating the region of
%interest in the given pictures.
RegionOfInterestSingleEvent(strtest3);

%
%Region of Image is the single variant of making a image calculation of the
%certain event.
RegionOfImage(str4, 'Visible', 'Slit')

%
%Code in process
PictureRectangles(str7, 'Calculate')

%
%PlotBurstTime is a script used to plot different time methods for a whole
%set of data. Tht means not just one day will be calculating and instead
%the whole map used. At this moment the code can only handle 4 months in
%this case September, October, November and December but improvement should work
%to do. See PlotBurstTime for more information.
% PlotBurstTime('FC', 'Hist')
% PlotBurstTime('Edge', 'Hist')
% PlotBurstTime('Corr', 'Hist')
%PlotBurstTime('Phase', 'ColorMap')
%PlotBurstTime('Edge-Corr', 'Scatter')
PlotBurstTime('Edge-FC', 'Scatter')
PlotBurstTime('Corr-FC', 'Scatter')
PlotBurstTime('Edge-Corr', 'Hist')

```

---

```

PlotBurstTime('Edge-FC', 'Hist ')
PlotBurstTime('Corr-FC', 'Hist ')
PlotBurstTime('FC', 'Hist ', 'Current ')
PlotBurstTime('FC', 'Hist ', 'Transmitted ')
PlotBurstTime('Corr', 'Hist ', 'Reflected ')
PlotBurstTime('Corr', 'Hist ', 'Input ')

PlotBurstTime('Image', 'Hist ', 'Interactive ')
PlotBurstTime('ImageEdge', 'Hist ', 'Interactive ')
PlotBurstTime('ImageCorr', 'Hist ', 'Interactive ')
PlotBurstTime('ImageFC', 'Hist ', 'Interactive ')

%%
%DoubleBDPlotter will plot all 16 signals that is given for 1 breakdown.
%Tis will be plotted for the breakdown and th 2 preceding normal logs. Same
%logs that is used for background calibration.
DoubleBDPlotter(str5)

```



# Bibliography

- [1] *A Multi-TeV linear collider based on CLIC technology: CLIC Conceptual Design Report*, edited by M. Aicheler, P. Burrows, M. Draper, T. Garvey, P. Lebrun, K. Peach, N. Phinney, H. Schmickler, D. Schulte and N. Toge, CERN-2012-007
- [2] *The CLIC Programme: towards a staged  $e^+e^-$  Linear Collider exploring the Terascale, CLIC Conceptual Design Report*, edited by P. Lebrun, L. Linssen, A. Lucaci-Timoce, D. Schulte, F. Simon, S. Stapnes, N. Toge, H. Weerts, J. Wells, CERN-2012-005
- [3] *CTF3 DESIGN REPORT*, edited by Edited by G. Geschonke (CERN) and A. Ghigo (INFN Frascati) CERN/PS 2002-008 (RF),CTF3 Note 2002-047,LNF-02/008 (IR), EUROPEAN ORGANIZATION FOR NUCLEAR RESEARCH,CERN - PS DIVISION
- [4] M.Jacewicz et al. *General-purpose Spectrometer for Vacuum Breakdown Diagnostics for the 12 GHz Test Stand at CERN*, <http://accelconf.web.cern.ch/AccelConf/IPAC2014/papers/thpme171.pdf>
- [5] M. Jacewicz, V. Ziemann, T. Ekelof, A. Dubrovskiy, R. Ruber *Spectrometers for RF breakdown studies for CLIC*,Uppsala University,CERN, Geneva, March 7 2016
- [6] M.Jacewicz et al. *UCXS Uppsala/CLIC X-Band Spectrometer, Crab cavity breakdown currents*,CERN 10/06/2015 [https://indico.cern.ch/event/388608/contributions/1820518/attachments/777050/1065589/jacewicz\\_presentation\\_cern\\_201506.pdf](https://indico.cern.ch/event/388608/contributions/1820518/attachments/777050/1065589/jacewicz_presentation_cern_201506.pdf), taken [18-05-2016].
- [7] M. Jacewicz, R. Ruber and V. Ziemann *Breakdown Tomography with Emitted Electrons,UCXS Uppsala/CLIC X-Band Spectrometer*,CLIC Workshop 19/01/2016, <https://indico.cern.ch/event/449801/>, Accessed [2016-05-25]
- [8] Benjamin J. Woolley. *High Power X-band RF Test Stand Development and High Power Testing of the CLIC Crab Cavity*, August 2015, <http://eprints.lancs.ac.uk/76926/> taken [2016-01-30].
- [9] Walter Wuensch. *High-Gradient Acceleration: CLIC and Beyond*,CLIC Workshop, 20 January 2016, [indico.cern.ch/event/449801/contributions/1945416/attachments/1214222/1772335/beyond\\_final.pdf](https://indico.cern.ch/event/449801/contributions/1945416/attachments/1214222/1772335/beyond_final.pdf) taken [2016-05-17].
- [10] Achard, C. and others, *30-GHz power production in CTF3*,Particle accelerator. Proceedings, Conference, PAC'05,Knoxville, USA, May 16-20, 2005,Conf. Proc, C0505161, 2005
- [11] Kovermann, Jan Wilhelm, *Comparative Studies of High-Gradient Rf and Dc Breakdowns*,CERN,2010,<http://inspirehep.net/record/914753/files/CERN-THESIS-2010-196.pdf>,CERN-THESIS-2010-196,
- [12] A. Descoeurdes, Y. Levinsen, S. Calatroni, M. Taborelli, W. Wuensch, *Investigation of the dc vacuum breakdown mechanism*. Physical Review Special Topics-Accelerators and Beams, vol. 12.9, no. 9, pp. 092001, (2009).
- [13] A.Degiovanni, W.Wuensch, and J.G.Navarro *Comparison of the conditioning of high gradient accelerating structures*, Phys. Rev. Accel. Beams 19, 032001 (2016) - Published 4 March 2016
- [14] W. Wuensch, *Introduction to the CLIC high-gradient development program*,mini-MeVArC, 21 March 2016, <https://indico.cern.ch/event/464716/>
- [15] Anders Korsback, Jorge Giner Navaro, Robin Rajamaki and Walter Wuensch *Statistics of breakdown and conditioning in pulsed dc and rf systems*,mini-MeVArC, 21 March 2016, <https://indico.cern.ch/event/464716/>

- [16] A.Palaia,V.Ziemann,R. Ruber, T.Ekelöf , *Beam momentum changes due to discharges in highgradient accelerator structures.*,ACTA UNIVERSITATIS UPSALIENSIS UPPSALA 2013,ISBN 978-91-554-8802-4, CLIC – Note – 1022
- [17] A. Degiovanni et.al *Diagnostics and analysis techniques for high power X-band accelerating structures*,Proceedings of LINAC 2014,Geneva,Switzerland,ISBN978-3-95450-142-7 490
- [18] E.Adli, *A Study of the Beam Physics in the CLIC Drive Beam Decelerator*, Department of Physics, University of Oslo, October 2009
- [19] V.Dolgashev, A.Haase, J.Lewandowski, G.Bowden, HZha, A.Grudiev, *Building Open Traveling Wave Accelerating Structure*, SLAC National Accelerator Laboratory and CERN Geneva Switzerland,International Workshop on Breakdown Science and High Gradient Technology(HG2015) 16-19 June 2015, Tsinghua University, Beijing , China
- [20] Robin Rajamäki, *Vacuum arc localization in CLIC prototype radio frequency accelerating structures*, Aalto University, 2016-04-04
- [21] J. Ögren, S. H. M. Jafri, K. Leifer, V. Ziemann, Uppsala University, Uppsala, Sweden *Surface characterization and field emission measurements of copper samples inside a scanning electron microscope*, Proceedings of IPAC2016, Busan, Korea Pre-Release Snapshot 19-May-2016, UTCMOPMR023



**LUND**  
UNIVERSITY

Series of Master's theses  
Department of Electrical and Information Technology  
LU/LTH-EIT 2016-548 <http://www.eit.lth.se>